ARMY RESEARCH LABORATORY

Investigation of a Bulk Metallic Glass as a Shaped Charge Liner Material

by William P. Walters, Laszlo J. Kecskes, and Justin E. Pritchett

ARL-TR-3864 **August 2006**

NOTICES

Disclaimers

Army Research Laboratory

Aberdeen Proving Ground, MD 21005-5066

ARL-TR-3864 **August 2006**

Investigation of a Bulk Metallic Glass as a Shaped Charge Liner Material

William P. Walters, Laszlo J. Kecskes, and Justin E. Pritchett
Weapons and Materials Research Directorate, ARL

REPORT DOCUMENTATION PAGE

Form Approved
OMB No. 0704-0188

1. REPORT DATE *(DD-MM-YYYY)*	2. REPORT TYPE	3. DATES COVERED (From - To)
August 2006	Final	May 2004 to December 2004

4. TITLE AND SUBTITLE
Investigation of a Bulk Metallic Glass as a Shaped Charge Liner Material

5a. CONTRACT NUMBER

5b. GRANT NUMBER

5c. PROGRAM ELEMENT NUMBER

6. AUTHOR(S)
William P. Walters, Laszlo J. Kecskes, and Justin E. Pritchett (all of ARL)

5d. PROJECT NUMBER
622105.AH84

5e. TASK NUMBER

5f. WORK UNIT NUMBER

7. PERFORMING ORGANIZATION NAME(S) AND ADDRESS(ES)
U.S. Army Research Laboratory
Weapons and Materials Research Directorate
Aberdeen Proving Ground, MD 21005-5069

8. PERFORMING ORGANIZATION REPORT NUMBER
ARL-TR-3864

9. SPONSORING/MONITORING AGENCY NAME(S) AND ADDRESS(ES)

10. SPONSOR/MONITOR'S ACRONYM(S)

11. SPONSOR/MONITOR'S REPORT NUMBER(S)

12. DISTRIBUTION/AVAILABILITY STATEMENT
Approved for public release; distribution is unlimited.

13. SUPPLEMENTARY NOTES

14. ABSTRACT

A study was conducted to explore a zirconium-based bulk metallic glass, Vitreloy 106, as a jetting material. In the past, bulk metallic glass alloys (e.g., Vitreloy 106) have been used for other applications such as the binder for kinetic energy penetrators. These alloys are a homogeneous mixture of several metals. Based on the experiments described herein, it was concluded that this zirconium-based bulk metallic glass behaves more like a shaped charge liner, which is fabricated from pressed powder metals, than a pure glass liner. In the extreme conditions during the formation and flight of the jet to the target, the bulk metallic glass liner disperses and its effectiveness is greatly diminished. It is conceivable that improvements in liner geometry, composition, and fabrication may result in an improved jet.

15. SUBJECT TERMS
bulk metallic glass; shaped charge

16. SECURITY CLASSIFICATION OF:			17. LIMITATION OF ABSTRACT	18. NUMBER OF PAGES	19a. NAME OF RESPONSIBLE PERSON
					William P. Walters
a. REPORT	b. ABSTRACT	c. THIS PAGE			19b. TELEPHONE NUMBER (*Include area code*)
Unclassified	Unclassified	Unclassified	SAR	45	410-278-6062

Standard Form 298 (Rev. 8/98)
Prescribed by ANSI Std. Z39.18

Contents

List of Figures

List of Tables

Acknowledgments

The authors would like to thank Mr. Kenneth Willison of the U.S. Army Armaments Research, Development, and Engineering Center, Picatinny Arsenal, New Jersey, for providing us with the metallic glass liners. We would also like to extend our thanks to Mr. Steven Aubert of the U.S. Army Research Laboratory (ARL) for performing the compatibility test between Vitreloy 106 and for loading the OCTOL[1] explosive charges as well. Additional kudos are due to Messrs. David Weeks, Jack Koontz, and the technical staff of experimental range facility 9. The authors further thank Mr. George Dewing of ARL for the sectioning and cleaning of the target plates, and Mr. Daniel Lozier of ARL for metallographicly preparing the the target sections. Special thanks to Amy Siegfried of ARL for assistance with figures 2 and 3; Ben Huntzinger of ARL for assistance with figure 9; and Richard Summers of ARL for an excellent technical review.

[1]OCTOL is a mixture of octogen and trinitrotoluene.

INTENTIONALLY LEFT BLANK.

1. Introduction

Vitreloy 106 is a zirconium-based bulk metallic glass (BMG) with an intended composition of $Zr_{57}Nb_5Cu_{15.4}Ni_{12.6}Al_{10}$, given in atomic percents, or $Zr_{67.95}Nb_{6.07}Cu_{12.79}Ni_{9.66}Al_{3.53}$ in weight percents. It has a density of 6.7 g/cm^3. With ultrasound measurements, it was determined that this BMG has a longitudinal wave velocity of 5350 m/s, a shear wave velocity of 2420 m/s, and thus a bulk sound velocity of 4562 m/s (*1*). For comparison, copper has a density of 8.9 g/cm^3 and a bulk sound velocity of 3980 m/s. At present, Vitreloy 106 and its higher density derivatives are candidate materials for use as the binder matrix for tungsten-reinforced composite kinetic energy penetrators. However, the material was never investigated regarding its potential use as a shaped charge liner material.

The use of a material as a shaped charge liner means that it will be subjected to extremely high strains, strain rates, pressures, and temperatures (*2*). In general, the behavior of any material during these conditions is not known. Historically, the best shaped charge liner materials are pure metals (*2*). On one hand, alloys of metals, with a few exceptions, do not form ductile coherent jets, and the jet is diffuse or spreads over time. On the other hand, jets that are fluid in nature do not particulate or break into particles as most metallic jets do. Simple oxide glass liners also perform well, but their penetration is low because of the low density of the jet. Shaped charge liners fabricated from pressed powders (usually a tungsten, copper, graphite mixture), as those used in the oil well industry, are coherent but tend to dissipate over time (*3*). For the oil well industry, this is not a major problem since the jet engages the target at short stand-off distance. Vitreloy 106 was assumed to behave somewhat like a powder liner because of its composition. The current study was an attempt to determine the exact nature of the jetting behavior from a shaped charge liner of Vitreloy 106.

2. Experimental Program

2.1 Shaped Charge Liner Geometry

Several conical shaped charge liners were fabricated by injection molding at Howmet Corporation (*4*) for the U.S. Armament Research, Development, and Engineering Center several years ago but were never tested. Two sets of liners were obtained from Howmet; one set was made from Vitreloy 1, and the other set was made from Vitreloy 106. Because Vitreloy 1 contains about 3 weight percent (wt %) beryllium, we decided not to test it as a shaped charge liner. Therefore, the study was conducted to determine the suitability of Vitreloy 106 as a possible jetting material only.

The conical liners were typically 86.9 mm (3.42 inches) in outer diameter with a nominal 42-degree apex angle. The liners had an altitude of 106.1 mm (4.178 inches). The conical liners had a cylindrical knob or plug at the apex which was 8.3 mm (0.325 inch) high and 12.8 mm (0.504 inch) in diameter. The liners proved to be "non-precision" in that the outer base diameter varied as much as 0.25 mm (0.01 inch) and the apex angle varied by as much as 0.5 degree among the three liners. Three Vitreloy 106 liners were available, and some were reported to have pores or voids near the apex but no macro flaws. This claim was not verified for each of the three liners. However, previously, a fourth Vitreloy 106 and another Vitreloy 1 liner were examined by X-ray radiography to detect pores, voids, or other flaws. As shown in figure 1, the primary flaw for the Vitreloy 106 liner (indicated by the red arrow and barely visible as a dark blemish) is concentrated at the plug at the apex of the cone. There are no apparent voids in the walls.

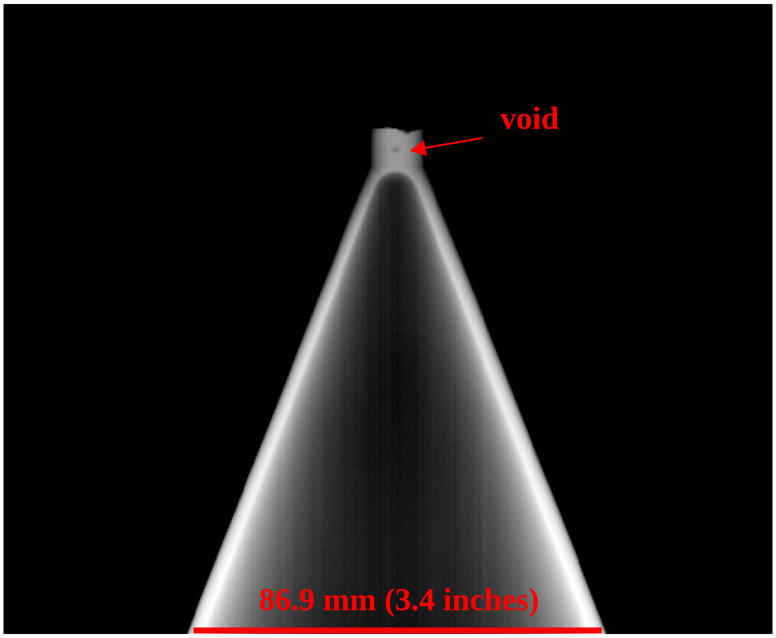

Figure 1. X-ray radiograph of a typical Vitreloy 106 shaped charge liner.

The wall thicknesses of the other liners were gauged and were again typical of a non-precision part. The wall thickness was measured every 90 degrees around the circumference of each liner and inward from the base. The wall thickness varied in the longitudinal and transverse planes. The typical uniform wall thickness was 3.25 mm (0.128 inch) or a 3.75% wall based on liner diameter. Tables 1 through 3 present the gauging data for each of the liners tested.

Table 1. Gauging data for liner 25.

Depth From Base Into Liner (mm)	0 degrees Wall Thickness (mm)	90 degrees Wall Thickness (mm)	180 degrees Wall Thickness (mm)	270 degrees Wall Thickness (mm)
At Base	3.327	3.251	3.327	3.327
19.050	3.327	3.251	3.327	3.378
22.225	3.327	3.251	3.353	3.378
25.400	3.302	3.251	3.353	3.378
34.925	3.251	3.175	3.353	3.378
41.275	3.251	3.150	3.353	3.378
44.450	3.175	3.150	3.353	3.302
50.800	3.175	3.099	3.353	3.302
63.500	3.175	3.124	3.378	3.302
73.025	3.175	3.124	3.480	3.327
76.200	3.175	3.150	3.480	3.378

Table 2. Gauging data for liner 18.

Depth From Base Into Liner (mm)	0 degrees Wall Thickness (mm)	90 degrees Wall Thickness (mm)	180 degrees Wall Thickness (mm)	270 degrees Wall Thickness (mm)
At Base	3.251	3.200	3.124	3.302
25.400	3.302	3.200	3.124	3.302
31.750	3.302	3.175	3.124	3.302
38.100	3.302	3.124	3.124	3.226
41.275	3.251	3.124	3.124	3.226
50.800	3.200	3.124	3.048	3.226
53.975	3.200	3.048	3.048	3.226
63.500	3.251	3.048	3.099	3.302
76.200	3.302	3.048	3.124	3.353

Outer diameter = 86.868 mm (3.420 inches); (1 inch = 25.4 mm).

Table 3. Gauging data for liner 23.

Depth From Base Into Liner (mm)	0 degrees Wall Thickness (mm)	90 degrees Wall Thickness (mm)	180 degrees Wall Thickness (mm)	270 degrees Wall Thickness (mm)
At Base	3.200	3.226	3.302	3.226
19.050	3.200	3.226	3.353	3.226
22.225	3.200	3.302	3.353	3.226
31.750	3.200	3.302	3.353	3.175
38.100	3.200	3.302	3.302	3.175
44.450	3.200	3.302	3.302	3.124
50.800	3.073	3.302	3.302	3.048
56.515	3.073	3.302	3.251	3.048
63.500	3.124	3.302	3.251	3.048
76.200	3.124	3.404	3.251	3.048

Outer diameter = 87.122 mm (3.430 inches); (1 inch = 25.4 mm).

2.2 Firing Program

The liners were loaded with 65/35 finely grained OCTOL[2] and were vacuum cast. The charge diameter was 101.6 mm (4.0 inches) and the cylindrical billet of OCTOL was 190.5 mm (7.5 inches) high. The total warhead weight varied from 2675 to 2780 g. The warhead did not have a case.

The first two shots were designed to determine the free-flight jet characteristics, and the final shot was for penetration. The tests were conducted at the experimental range facility (ERF)-9 at the U.S. Army Research Laboratory (ARL). ERF-9 used two 150-kilo-electron-volt (keV) X-rays for the early flash times with orthogonal flashes and three 450-keV X-rays for the later times.

Shot 3618 had flash times, measured from the detonator, of 58.14 µs for the orthogonal flashes, and 74.18, 174.16, and 274.44 µs for the later flash times.

Liner 23 was the first round tested. The warhead weight was 2780 g. Figure 2 shows the location of the charge in a protective barbette (the charge was located 12.7 mm (0.5 inch) behind the edge of the barbette) and the relative distances to the X-ray tube heads. The barbette, which surrounds the charge, is on the right, and the witness pack (residual armor) is on the far left. The result was a splatter on the first witness plate.

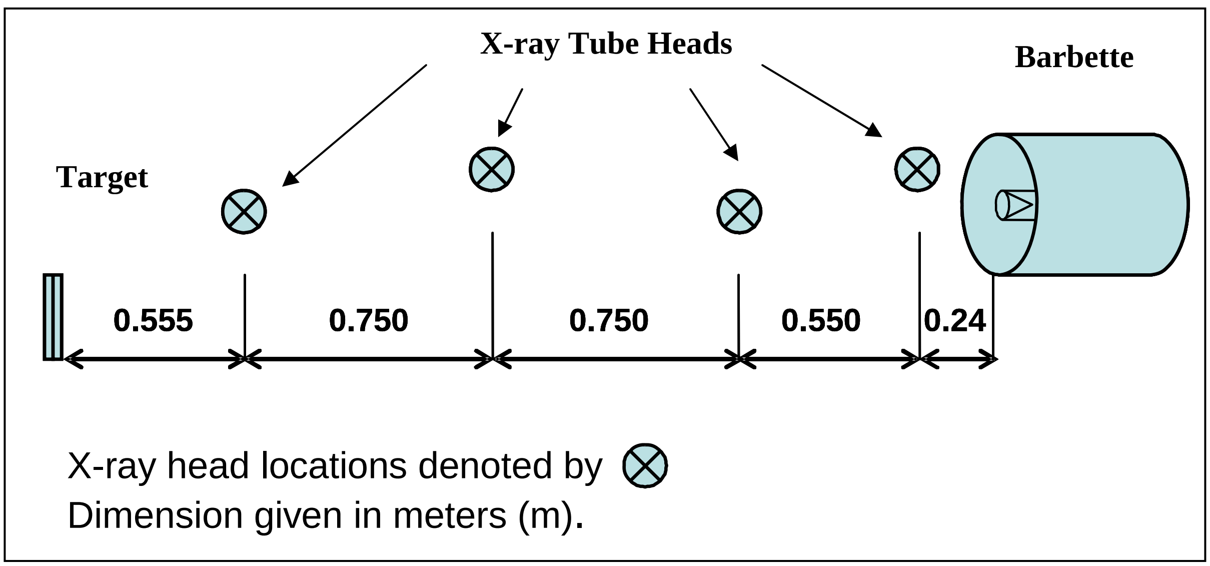

Figure 2. Schematic of the test setup for shot 3618. (Shot 3618 was performed September 21, 2005 at EF-9. Charge 23 had a charge mass of 2780 g. Stand-off distance was 2845 mm. Charge location was 12.7 mm [0.5 inch] behind the edge of the barbette.)

Shot 3619 was the second free-flight radiography test designed to examine the jet more closely now that the tip velocity was accurately known. This test used liner 25 and the warhead weight was 2675 grams. The variation in warhead weight from liner 23 was attributable to the lack of precision in the liner. Figure 3 shows the location of the charge in a protective barbette (the charge

[2]OCTOL is a mixture of octogen (cyclotetramethylene-tetranitramine) and trinitrotoluene.

was located 63.5 mm (2.5 inches) behind the edge of the barbette) and the distances to the x-ray heads. The flash times were 67.1, 124.2, 149.3, and 174.5 μs. The barbette, which surrounds the charge, is on the right, and the witness pack (residual armor) is on the far left. The result was perforation of the first witness plate.

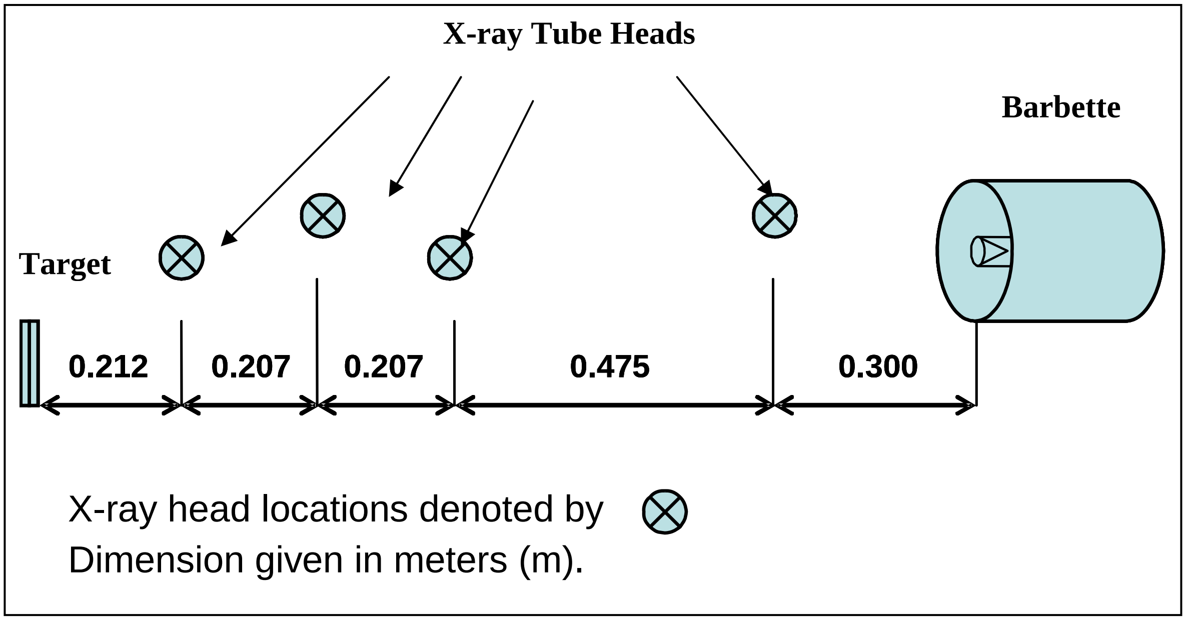

Figure 3. Schematic of the test setup for shot 3619. (Shot 3619 was also performed September 21, 2005 at EF-9. Charge 25 had a charge mass of 2675 g. Stand-off distance was 1401 mm [55 inches]. Charge location was 63.5 mm [2.5 inches] behind the edge of the barbette.)

The final shot 3620 was designed only for penetration at a shorter stand-off distance. Again, the witness plates (target) consisted of a stack of 25.4-mm-thick (1-inch-thick) rolled homogeneous armor (RHA) plates. The stand-off distance was 203.2 mm (8 inches) or two charge diameters (CDs).

2.3 Sample Analysis

After the completion of the three firing tests, the plates were photographed and sectioned to examine the interaction surface between the steel and the Vitreloy 106 liner material. Sectioned pieces were further cut, cleaned of rust, and sequentially polished for scanning electron microscopy and trace elemental identification by energy dispersive X-ray analysis.

3. Results and Discussion

3.1 Jet Radiography and Overall Target Plate Appearance

3.1.1 Shot 3618

The flash radiographs from shot 3168 are shown in figures 4 and 5. In figure 4, the jet travels from right to left. The first appearance of the jet at the earliest flash time shows the jet with a large bulb-like tip. In the next flash, the jet bifurcates or comes apart at the tip and begins to dissipate at later times. At the last or longest flash time, 274.44 µs, the jet nearly disappears. This is typical of powder jets. Figure 5 shows an enlarged version of the jet, at 74.18 µs. There were gaps or hollow regions in the jet which may indicate the presence of voids in the liner. Another effect of void or non-uniformity in the cast liner is manifested in the large variation of particulate size in the jet. The stand-off distance was 2845 mm or 28 CD and the penetration was small. The jet impacted the lower left-hand corner of the witness plate and the maximum hole depth was 19 mm. The jet tip velocity was measured to be 8.3 km/s.

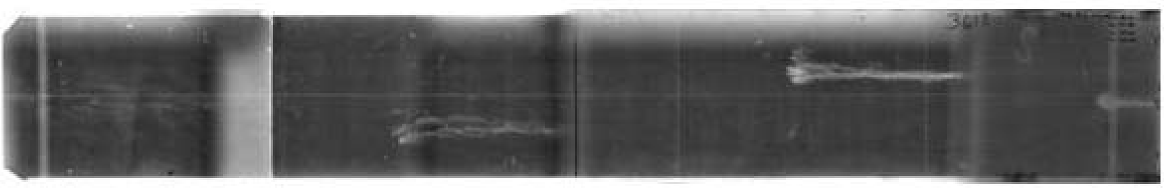

Figure 4. Multi-exposure flash x-ray radiograph of shot 3618.

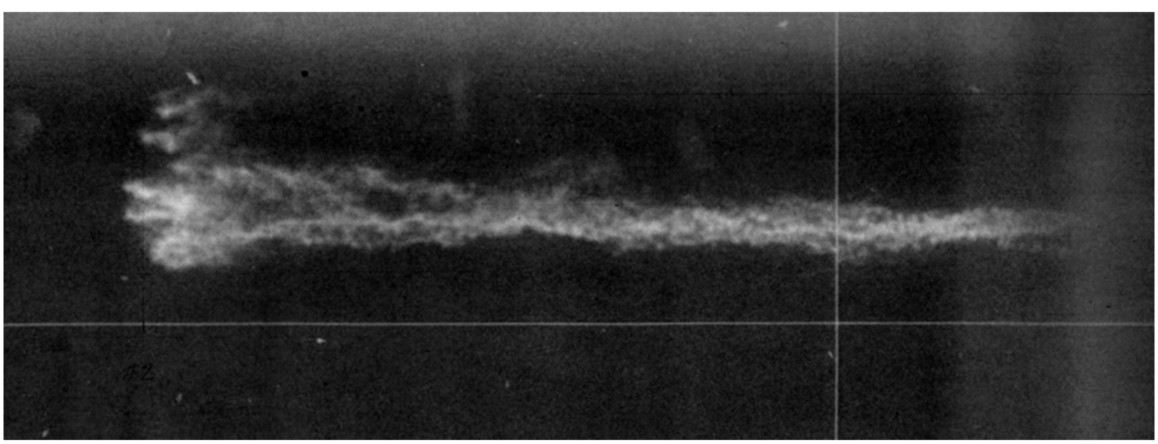

Figure 5. Key section of the jet from shot 3618. (Note the extensive particulation, dispersion, and diffusion of the jet.)

This result is consistent with the flash X-ray in that the jet was not straight and was diffuse. Figure 6 shows the impact region 6(a) on the first witness plate. The lack of any bulging on the

rear of the plate, shown in 6(b), testifies to the incompleteness of the penetration into the plate. As apparent, very little penetration was observed. It is difficult to discern the damaged region of the front side of the plate in the macro photographs. Note the bluish-black discoloration of the impacted surface. Figure 7 shows a closer view of the sectioned lower left corner with a clear demonstration of fragments peppering the plate surface without any appreciable penetration.

A higher magnification view of the damaged surface is shown in figure 7. The random pitting pattern is caused by the incoherent jet breaking into fragments and impacting the plate surface. Most of the pits are shallow and about 1 to 3 mm in diameter, although some of the pits are larger (12 to 15 mm in diameter). In some cases, the pit damage overlaps. Proportional to their size, the corresponding pits are also deeper. The bluish discoloration is from staining and adhesion of possibly molten liner material. The surface erosion is uneven. Generally, the larger pits contain liner material.

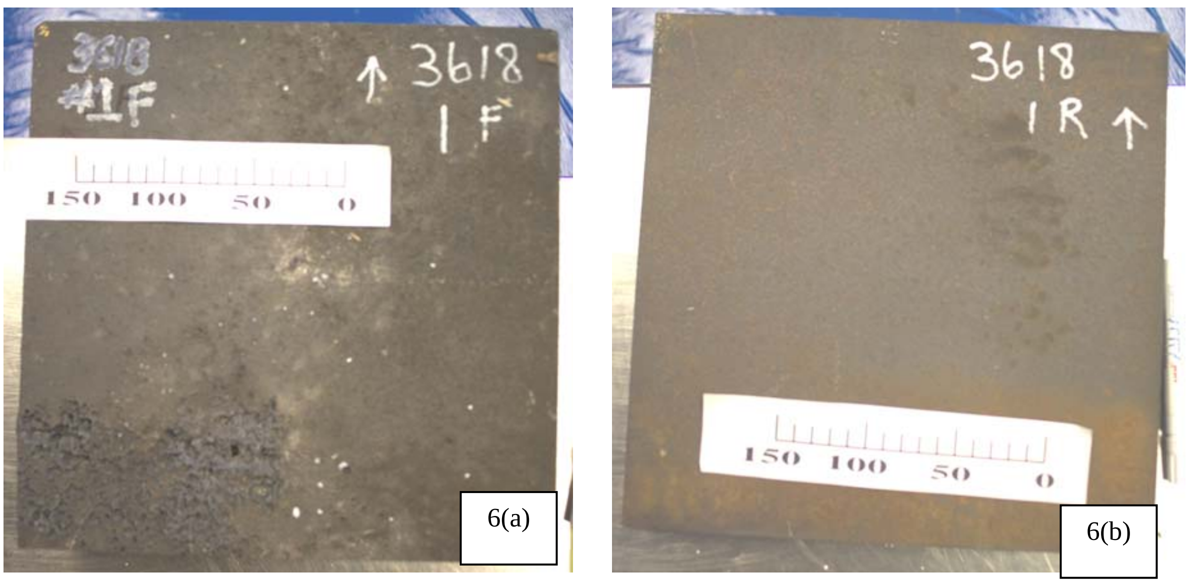

Figure 6. First witness plate for shot 3618 with its front shown in 6(a) and rear shown in 6(b).

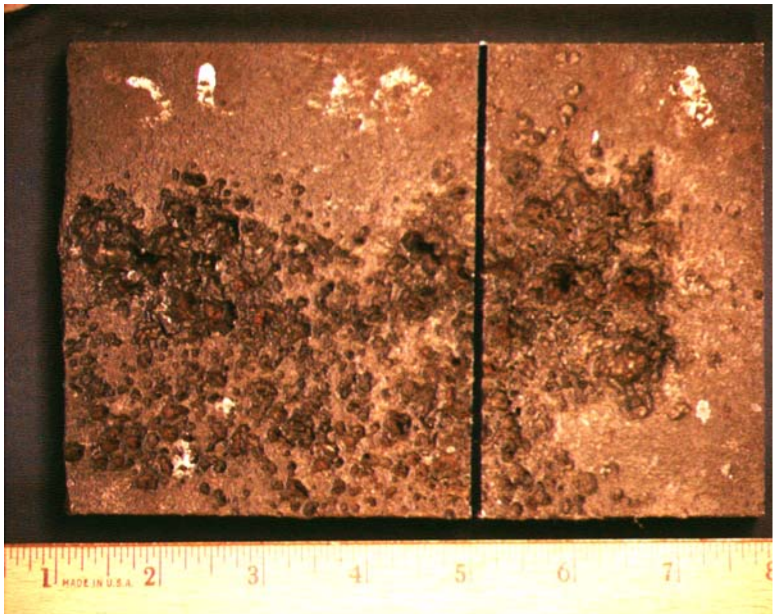

Figure 7. Closer view of the lower left corner of the first witness plate for shot 3618.

3.1.2 Shot 3619

Figure 8 shows the flash radiographs of the jet from shot 3619. Again, the jet exhibits a “powdery” appearance with evidence of voids in the jet. The jet dissipates at later times and is not straight. The stand-off distance was lowered to 1401 mm or 13.8 charge diameters. The penetration was greater than 25.4 mm (1-inch), i.e., the jet penetrated the first 1-inch-thick witness plate and entered the second plate. The depth of the hole in the second plate was about 15 mm. Figure 9 shows the measured hole profiles. Note that the hole shape is irregular because of the diffuse nature of the jet. Also, multiple impacts are present because of the bifurcation of the jet. Figure 10(a) through (d) show the macro photographs of the entrance and exit holes from both plates.

Figure 11(a) through (b) show close views of the hole patterns in the first and second witness plates, as well as higher magnification views of the interior of the cavity walls (figure 11[c] through [h]) in the front plate after it was sectioned. The inside surface of the wall is quite rough with clear evidence of liner material adhering to it. There is no discoloration of the very small pits, less than 3 mm in diameter. Fine blue-colored debris is found to coat the walls of the very large holes in the first witness plate. The cavities in the second plates are similar and small, blue particle remnants are found at their bottoms.

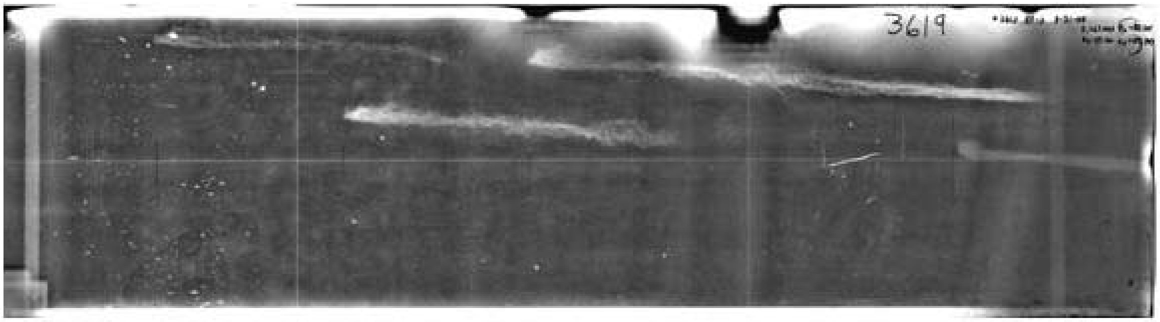

Figure 8. Multi-exposure flash x-ray radiograph of shot 3619.

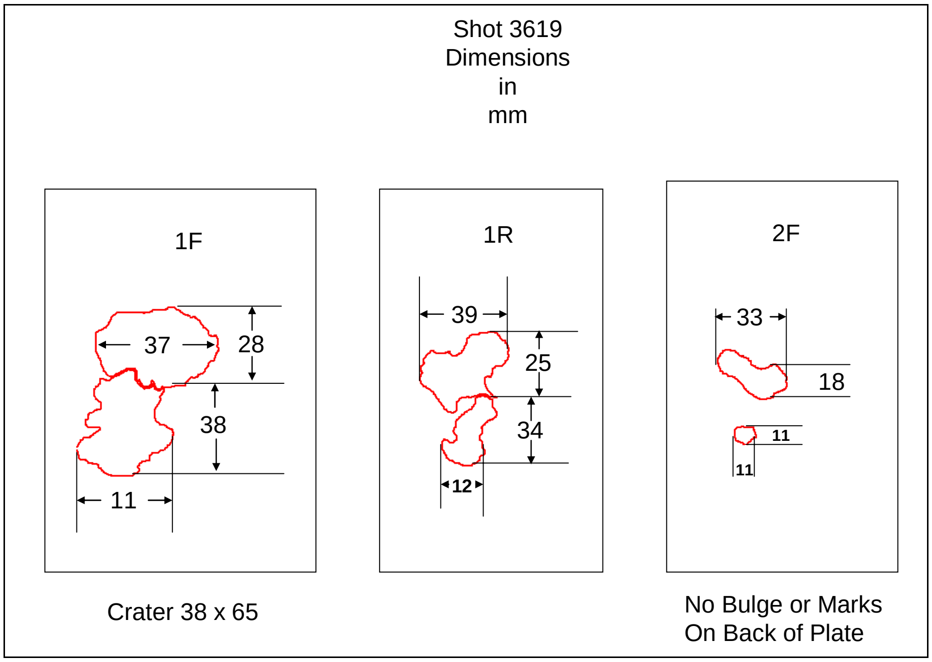

Figure 9. Hole geometry for shot 3619.

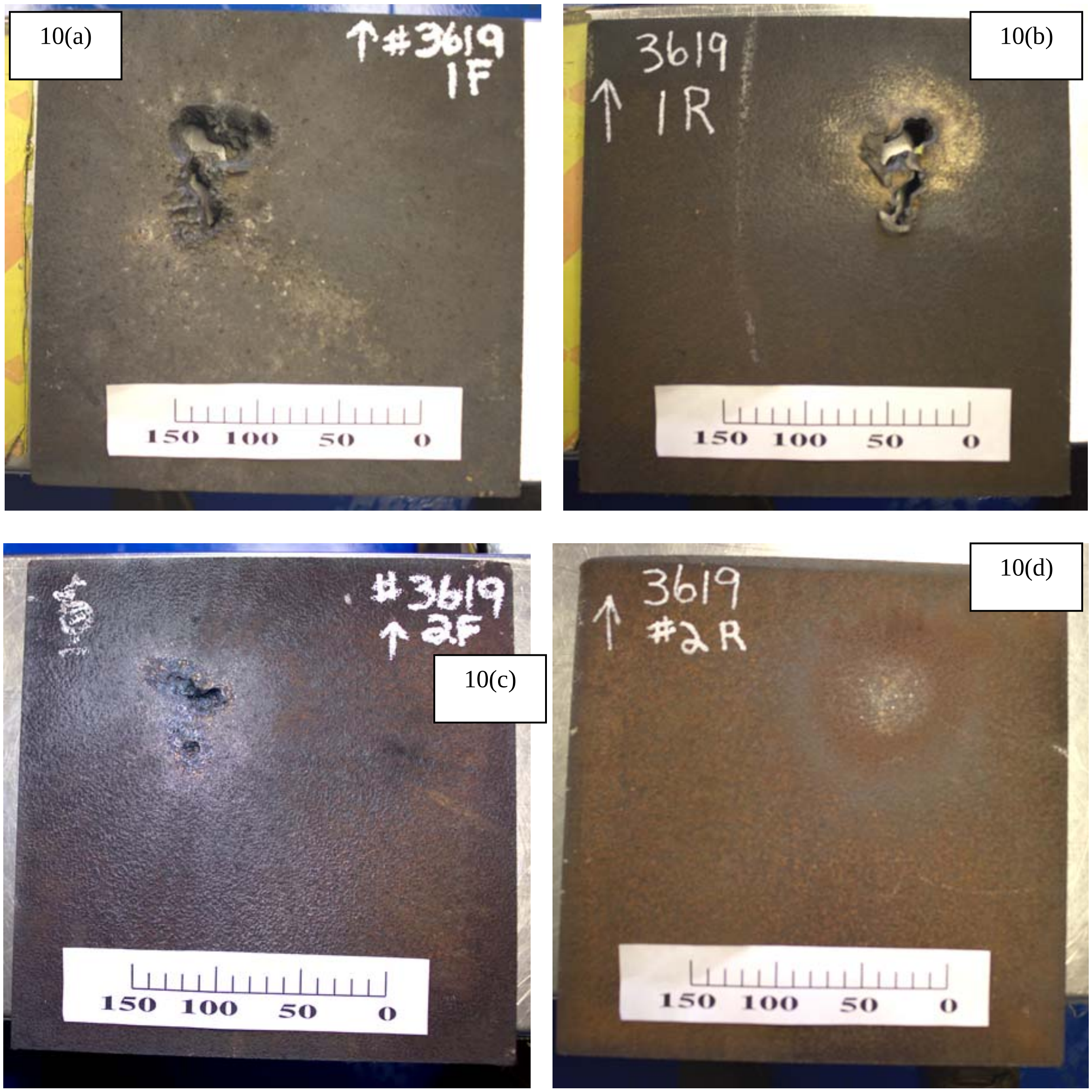

Figure 10. Entrance and exit hole macro photographs for shot 3619. (Figure 10(a) and (b) show the front and rear of the first witness plate, respectively. Figure 10(c) and (d) show the front and rear of the second witness plate, respectively. Note again the bluish discoloration from the liner residue adhering to the surface.)

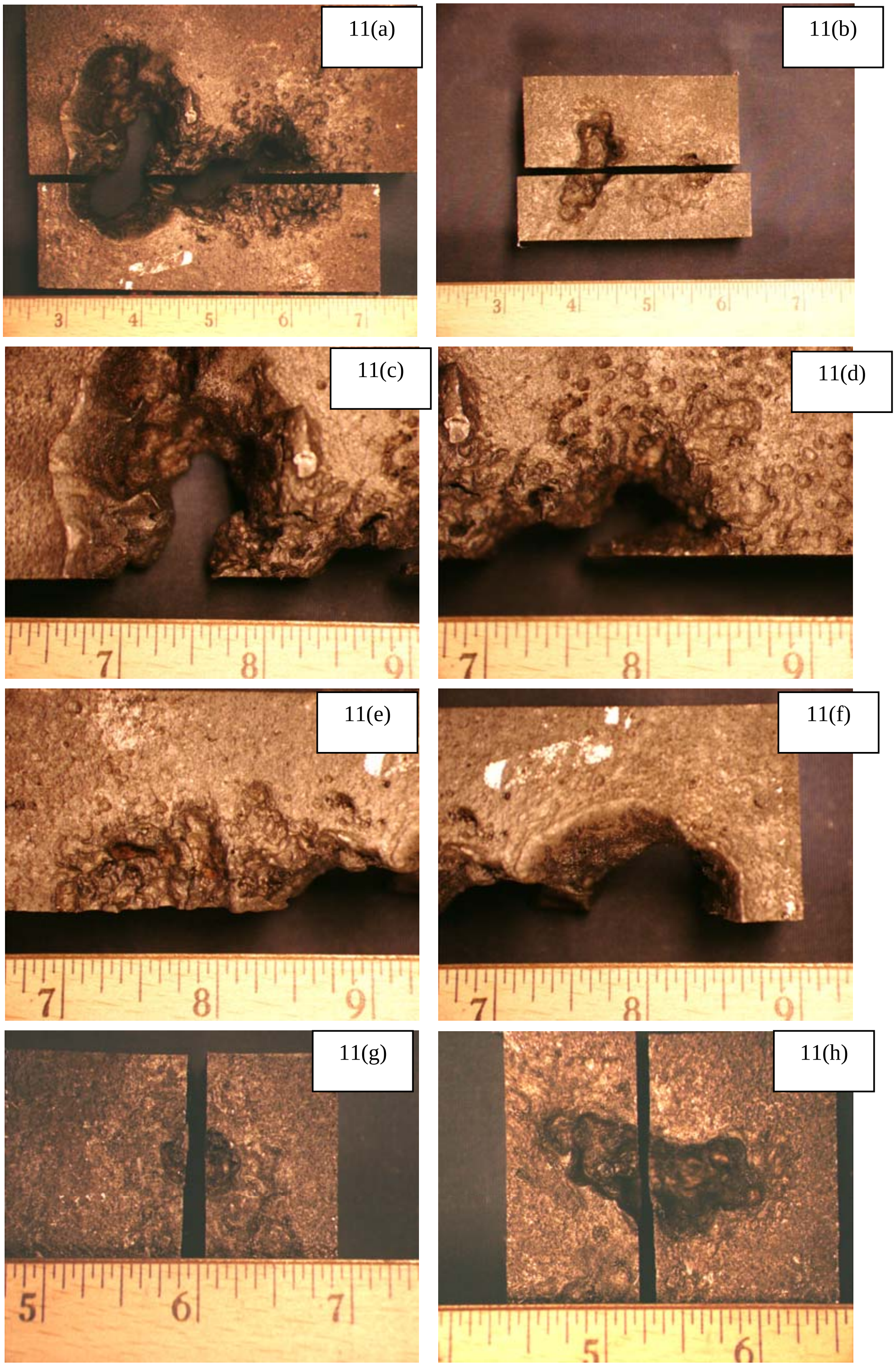

Figure 11. Closer view of the entrance holes into the two witness plates from shot 3619. (Figure 11(a) and (b) provide an overview of the hole in the first plate and the partially penetrated second plate. Figure 11(c), (d), (e), and (f) magnify the damage to the first plate. Figure 11(g) and (h) show the partial penetration to the second plate.)

3.1.3 Shot 3620

In the final shot 3620, the jet penetrated nine 25.4-mm (1-inch) plates and 4 mm into the tenth plate for a total penetration of 232.6 mm (9.16 inches) or 2.3 CD. This penetration depth is not impressive but indicative of powder jets in that the best penetration is achieved at short standoff. Table 4 lists the hole profile data and figures 12 through 21 display photographs of the entrance and exit holes for each witness plate. The entrance hole (first target plate) was relatively large (about 52.0 mm [2 inches]), and the holes were nearly circular.

Table 4. Hole profile data for shot 3620.

Plate Number		X(mm)	Y(mm)
1	Entrance	57	52
	Exit	33	32
2	Entrance	33	26
	Exit	28	29
3	Entrance	24	28
	Exit	28	29
4	Entrance	20	19
	Exit	27	28
5	Entrance	18	20
	Exit	28	23
6	Entrance	20	12
	Exit	24	17
7	Entrance	13	13
	Exit	21	23
8	Entrance	13	14
	Exit	15	15
9	Entrance	15	15
	Exit	8	10
10	Entrance	12	13 (4 mm penetration)
	Exit	0	0

Examination of the hole profiles in each of the target plates revealed that unlike those seen in the previous two shots, the last shot produced a considerably smoother surface finish. Moreover, while the erosion surfaces were again discolored, the coloration was less intense, indicative of less residual Vitreloy 106 liner material adhering to the walls. The plates were cut and figures 22 and 23 illustrate the penetration profile of the jet. A closer view of each of the witness plates is provided in appendix A.

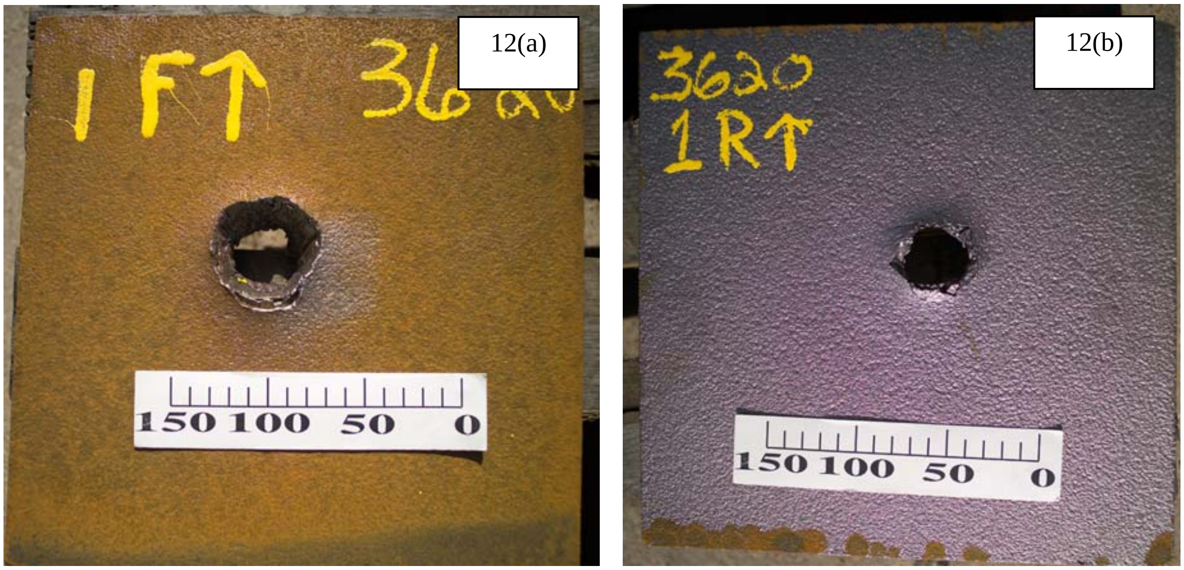

Figure 12. Entrance 12(a) and exit 12(b) holes of the first witness plate.

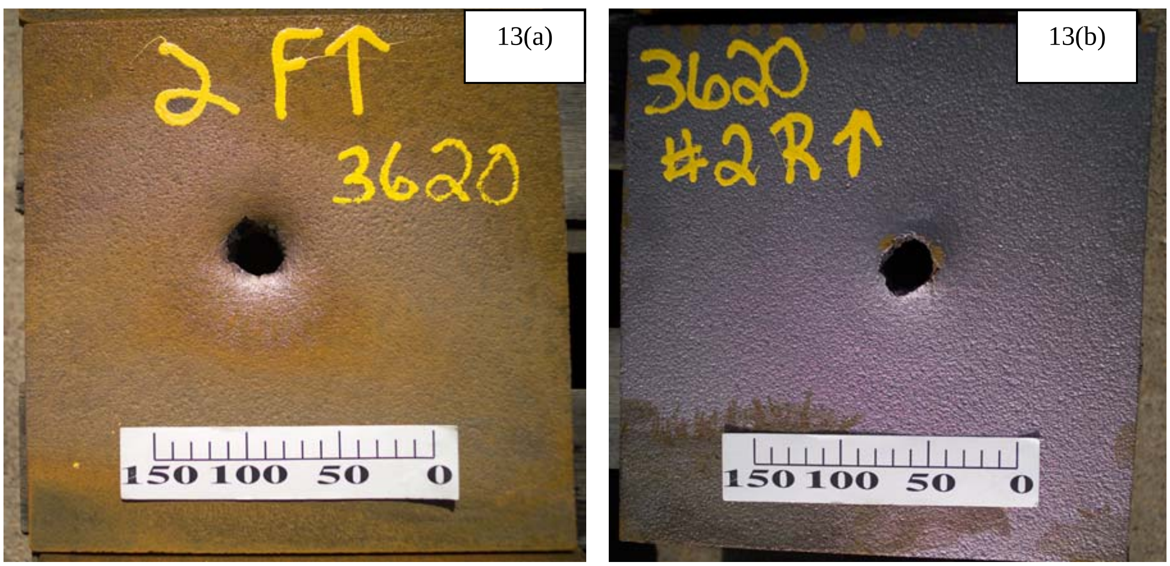

Figure 13. Entrance 13(a) and exit 13(b) holes of the second witness plate.

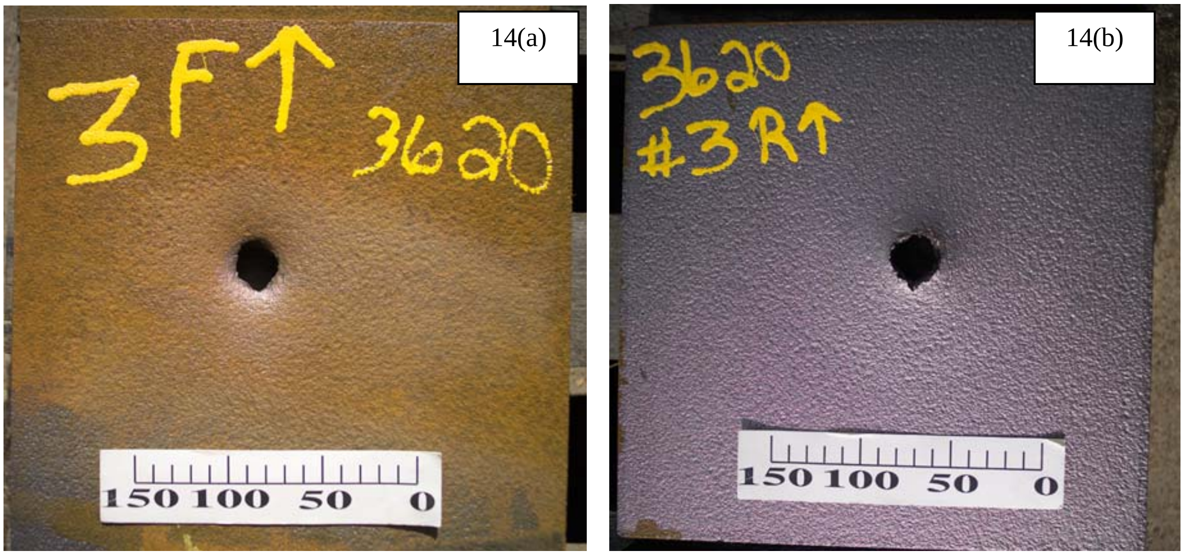

Figure 14. Entrance 14(a) and exit 14(b) holes of the third witness plate.

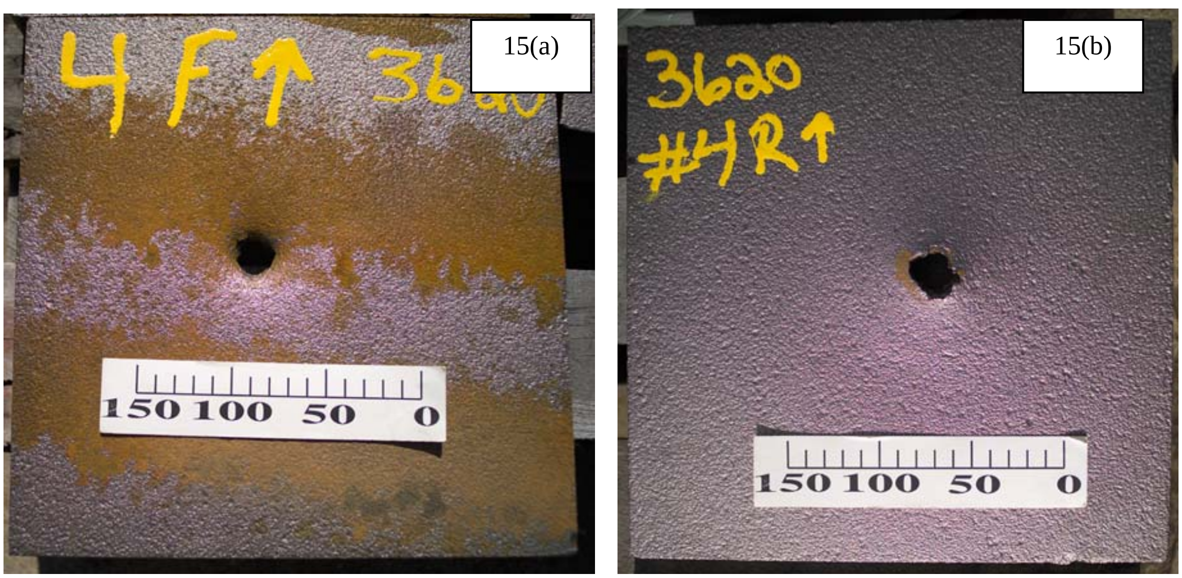

Figure 15. Entrance 15(a) and exit 15(b) holes of the fourth witness plate.

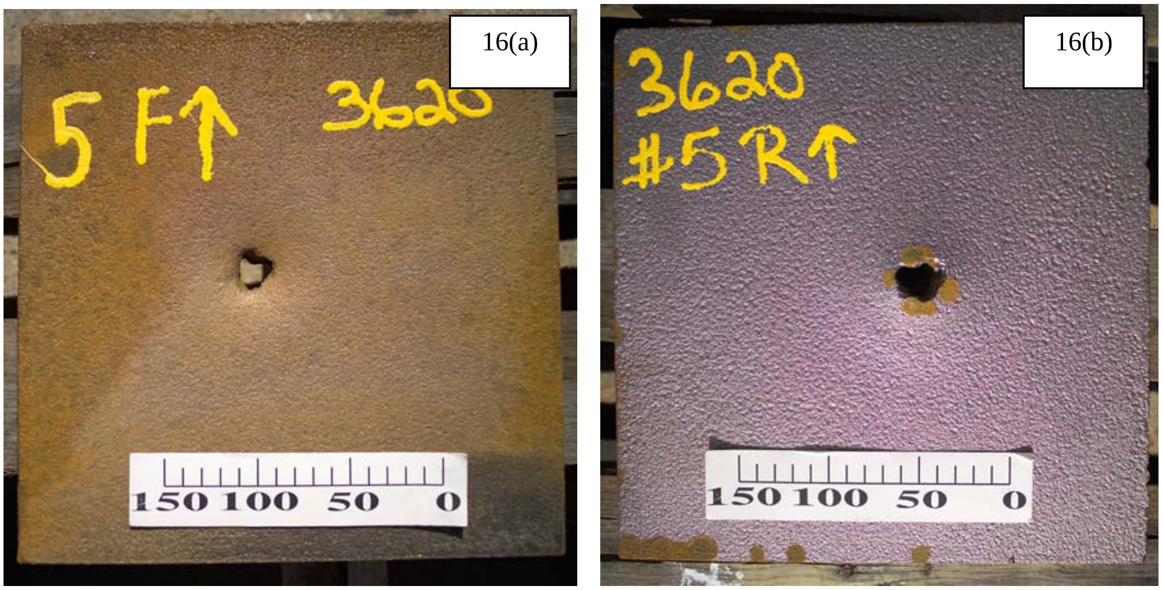

Figure 16. Entrance 16(a) and exit 16(b) holes of the fifth witness plate.

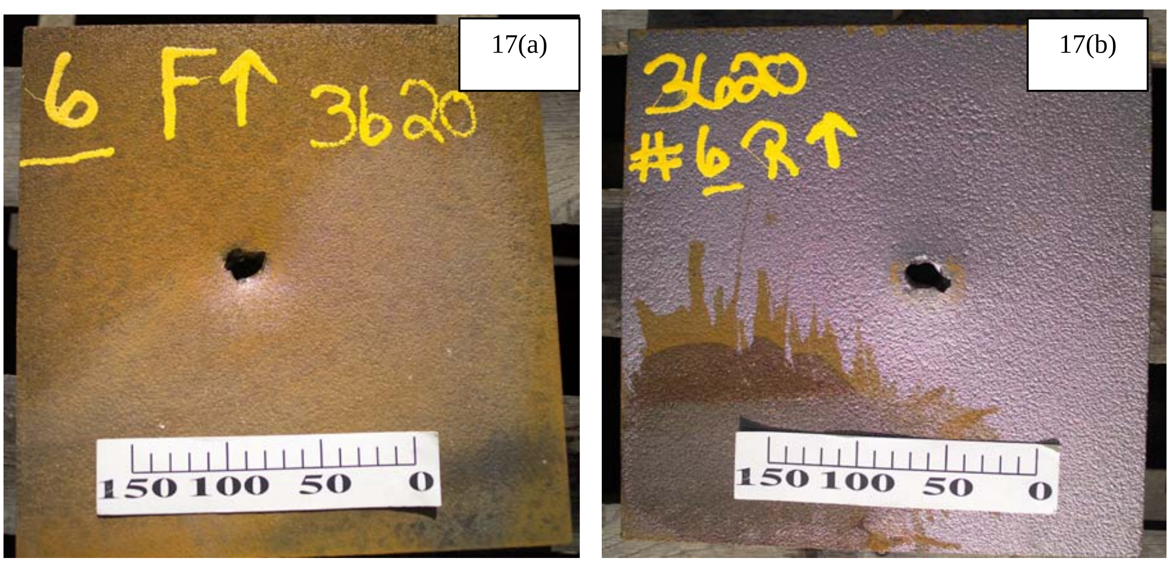

Figure 17. Entrance 17(a) and exit 17(b) holes of the sixth witness plate.

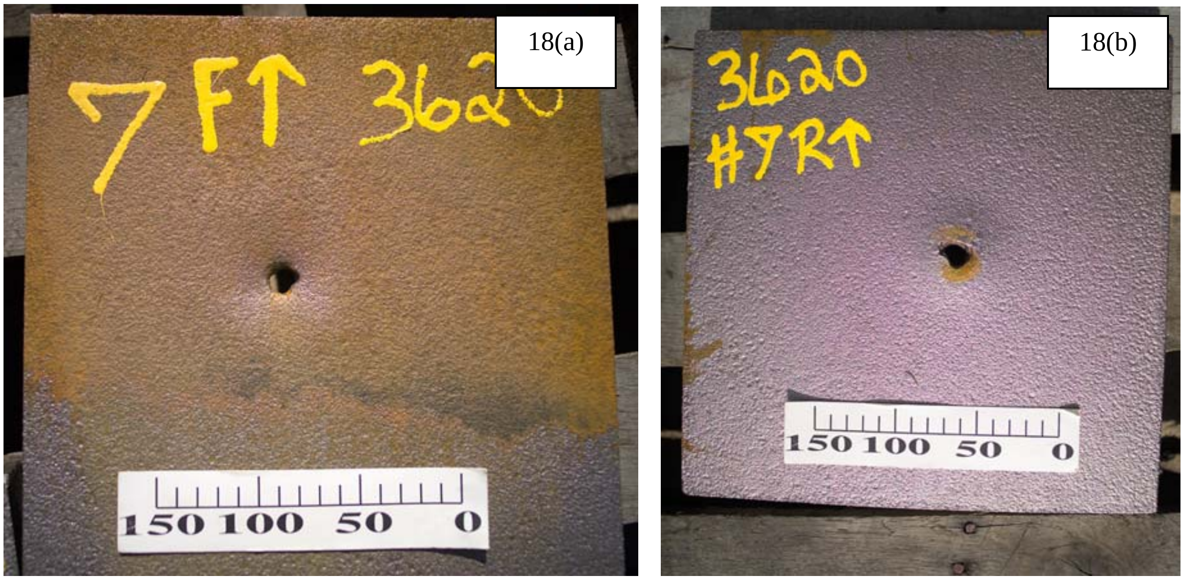

Figure 18. Entrance 18(a) and exit 18(b) holes of the seventh witness plate.

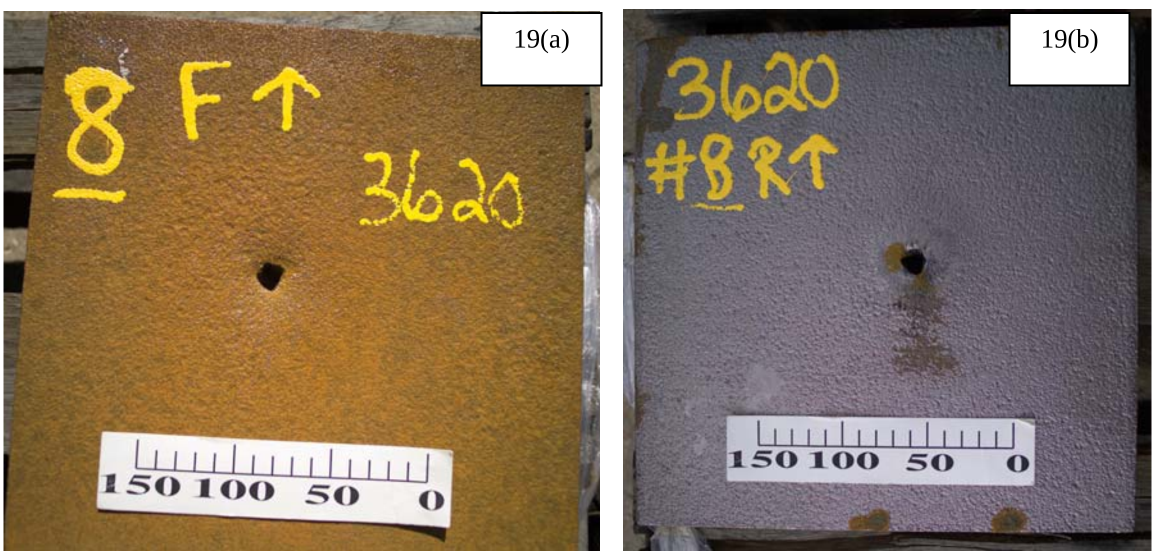

Figure 19. Entrance 19(a) and exit 19(b) holes of the eighth witness plate.

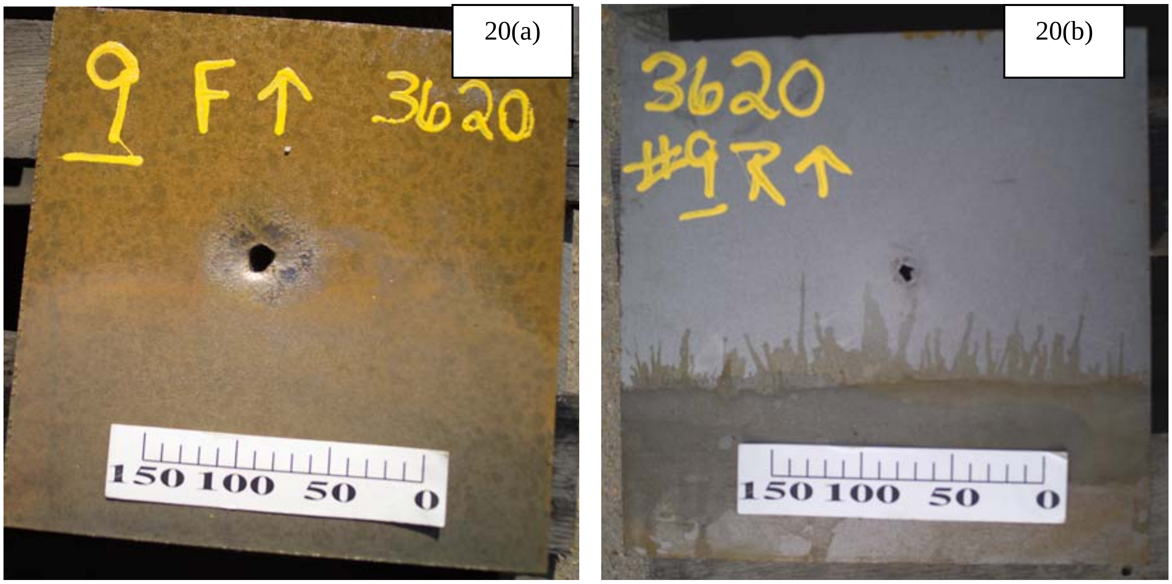

Figure 20. Entrance 20(a) and exit 20(b) holes of the ninth witness plate.

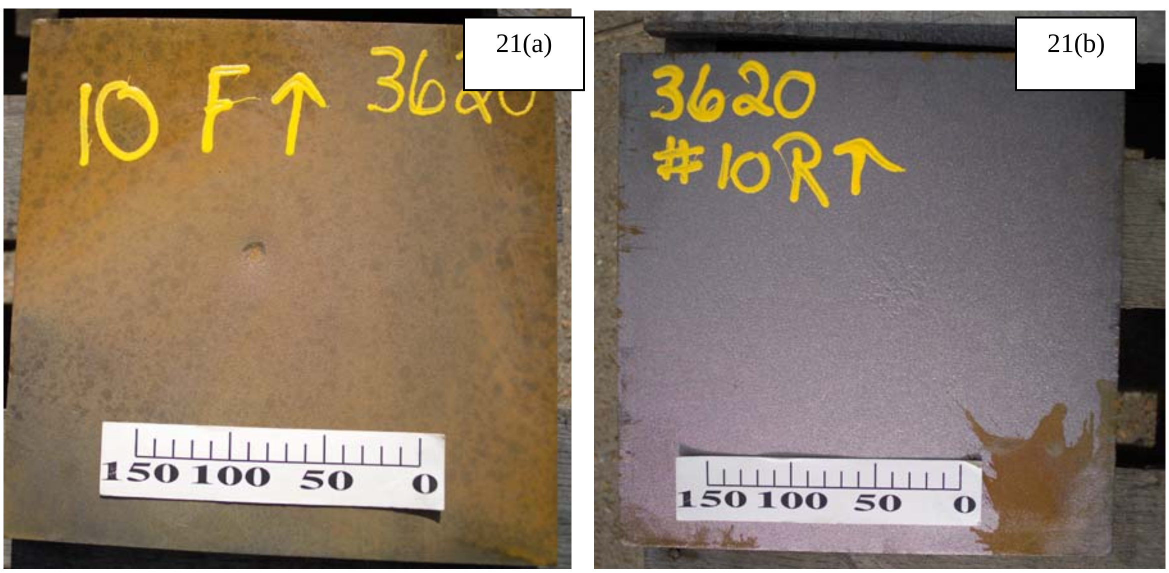

Figure 21. Entrance 21(a) and exit 21(b) holes of the tenth witness plate.

Figure 22. Side A of the cross-sectional view of the target block showing the penetration profile produced by the Vitreloy 106 shaped charge.

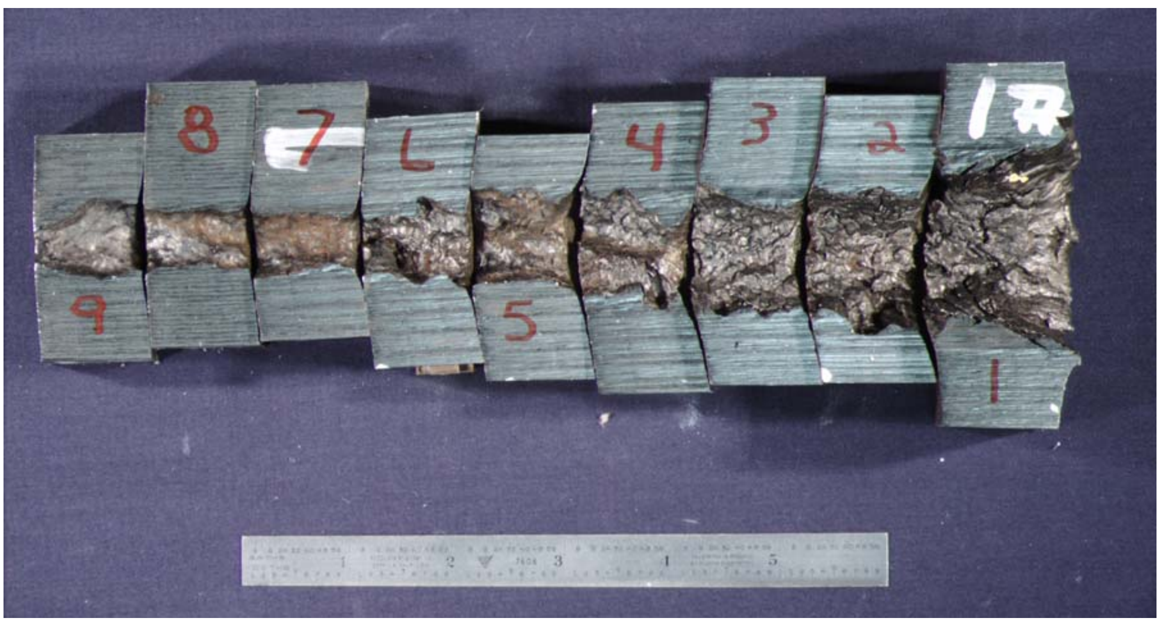

Figure 23. Side B of the cross-sectional view of the target block showing the penetration profile produced by the Vitreloy 106 shaped charge.

3.2 Analysis of the Target Plate Surfaces

A small section from one of the Vitreloy 106 liners was subjected to chemical analysis to verify its compositional integrity and detect any impurities that may affect its glass-forming ability. It is well known that oxygen and carbon interstitials in a bulk metallic alloy strongly affect how readily the alloyed bulk material can be quenched into a vitreous state (*5*). Table 5 presents the

intended and measured atomic and weight fraction of the elements in the metallic glass liner. All metallic elements were measured with direct current plasma emission spectroscopy, carbon with combustion infrared detection, whereas oxygen and nitrogen were measured with inert gas fusion.

Table 5. Elemental analysis of line 18.

Element	Intended Composition (Atomic %)	Actual Composition (Atomic %)	Intended Composition (Weight %)	Actual Composition (Weight %)
Zirconium	57	50.4	67.95	63.0
Niobium	5	3.10	6.07	3.95
Copper	15.4	15.7	12.79	13.7
Nickel	12.6	13.1	9.66	10.5
Aluminum	10	14.1	3.53	5.22
Oxygen	-		-	0.076
Nitrogen	-		-	0.007
Carbon	-		-	0.025
Titanium	-	2.06	-	1.35
Hafnium	-	0.009	-	0.023

Vitreloy 106 has an intended composition of $Zr_{57}Nb_5Cu_{15.4}Ni_{12.6}Al_{10}$, given in atomic percents, or $Zr_{67.95}Nb_{6.07}Cu_{12.79}Ni_{9.66}Al_{3.53}$ in weight percents. As the chemical analysis shows, the liner only marginally meets the intended composition. Trace quantities of Ti and Hf were detected, and considerable amounts of the interstitials were found as well.

After the witness plates from the experimental program were sectioned, regions near the erosion surfaces and underlying steel substrates were examined with scanning electron microscopy and energy dispersive X-ray spectroscopy.

Results show that in the first two experimental shots, early dispersion of the jet during the initial collapse and flight caused the Vitreloy 106 alloy material to be less effective by the time it reached the target stack (witness plates). Consequently, in shot 3618, most of the damage was imparted to the shallow top layer of the first witness plate, with relatively little erosion and minor pitting only. Small pits were either empty or discolored with a thin coating of the Vitreloy 106. Generally, deeper pits contained small but heavily oxidized liner fragments.

The depth of penetration from the liner in shot 3619 was much improved. The damage was more extensive, but the appearance of the affected surfaces was similar to those described previously. Additionally, some of these fragments had rounded edges and a molten appearance. Finer particulate debris was found to adhere on larger erosion surfaces. These surfaces were clearly a result of a combination of particulate erosion, impact, and dynamic flow.

Unlike the first two diagnostic tests, the third test, shot 3620, generated much smoother erosion surfaces. Although no large-scale debris or particulate matter was found on these surfaces, the tell-tale bluish discoloration was still present. Regions from witness plates A-2, A-3, and A-8 of figure 22 were scrutinized to a greater extent. (See appendix A for a close view of each sectioned witness plate.)

In this shot, by the elimination of the large stand-off distance, excessive dispersion of the liner material was circumvented. Consequently, more of the kinetic energy was converted into penetration. As the jet particulates erode the surface and come to rest in the target cavity because of subsequent latent heating in the target and depending on the available heat, the metallic glass undergoes partial or complete melting. Typically, when a vitrified metallic glass is heated above its glass transition temperature, its viscosity decreases several orders of magnitude. Then, it is not unreasonable to expect that this viscous solid could easily flow over the free surface of the steel target. As presented in figures 24 through 27, in certain areas, the bulk metallic glass liner at some time flowed, coated, and alloyed with the steel witness plate. In such a region, following this erosion process, the molten and resolidifying metallic glass intermixed and alloyed with the steel. The intermixed region contained voids and mostly large crystalline structures. Qualitative analysis of this intermixed region on the surface consisted of the elemental components of the bulk metallic glass and steel. Within the alloy material, there was less iron present, whereas, in the subsurface steel region, analysis revealed iron and manganese, consistent with the composition of the RHA plate. Note the presence of cracks along the interface between intermix region and the primary metallic glass layer that likely formed because of the strong differences between thermal properties of the materials during cooling.

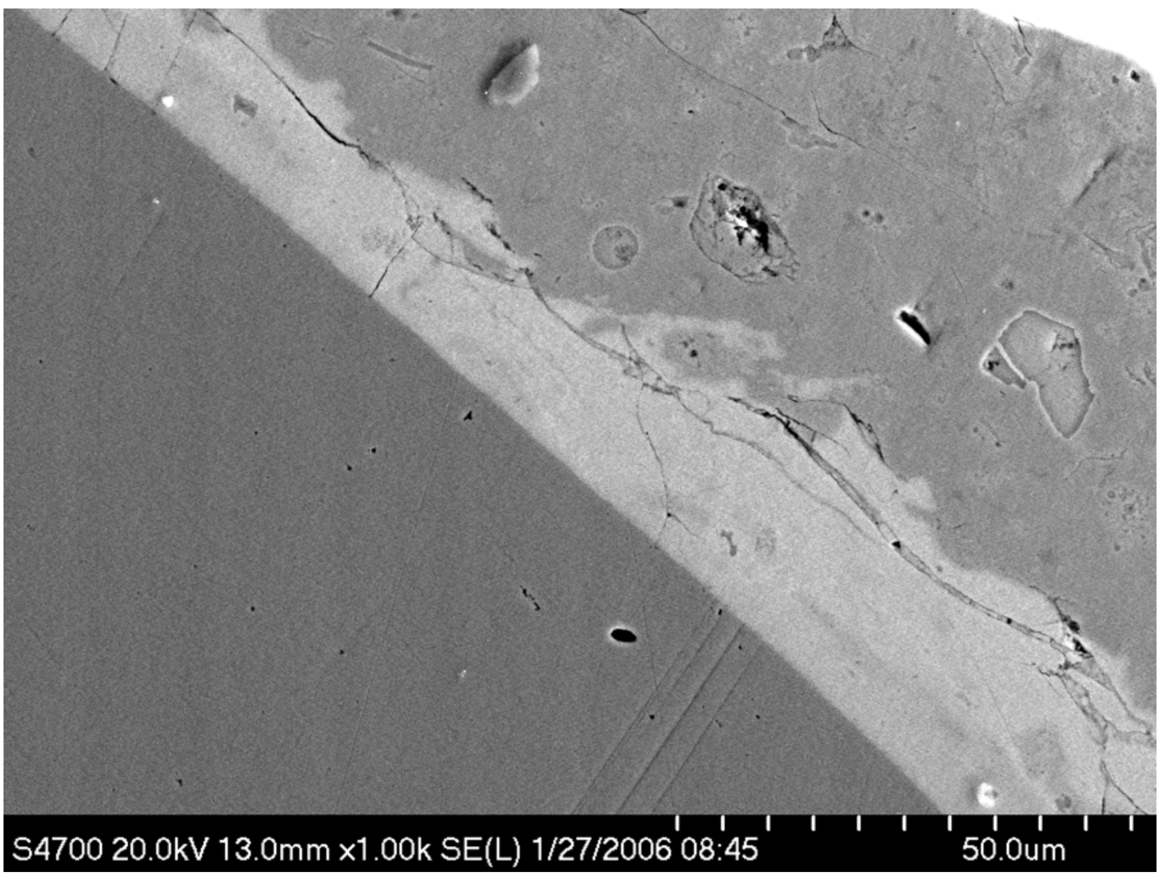

Figure 24. Secondary electron micro graph of a subsurface region of the A-2 witness plate is displayed.

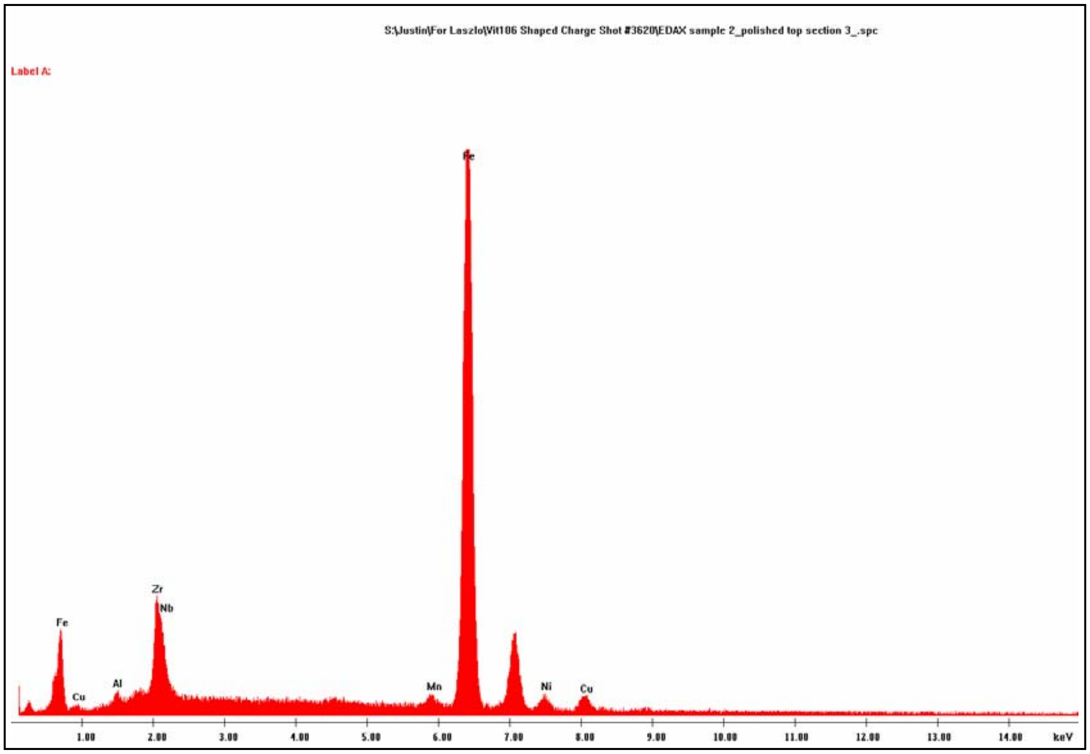

Figure 25. Secondary electron micro graph of a subsurface region of the A-2 witness plate displayed in figure 24, with the corresponding energy dispersive X-ray spectroscopic analyses for the top intermix layer.

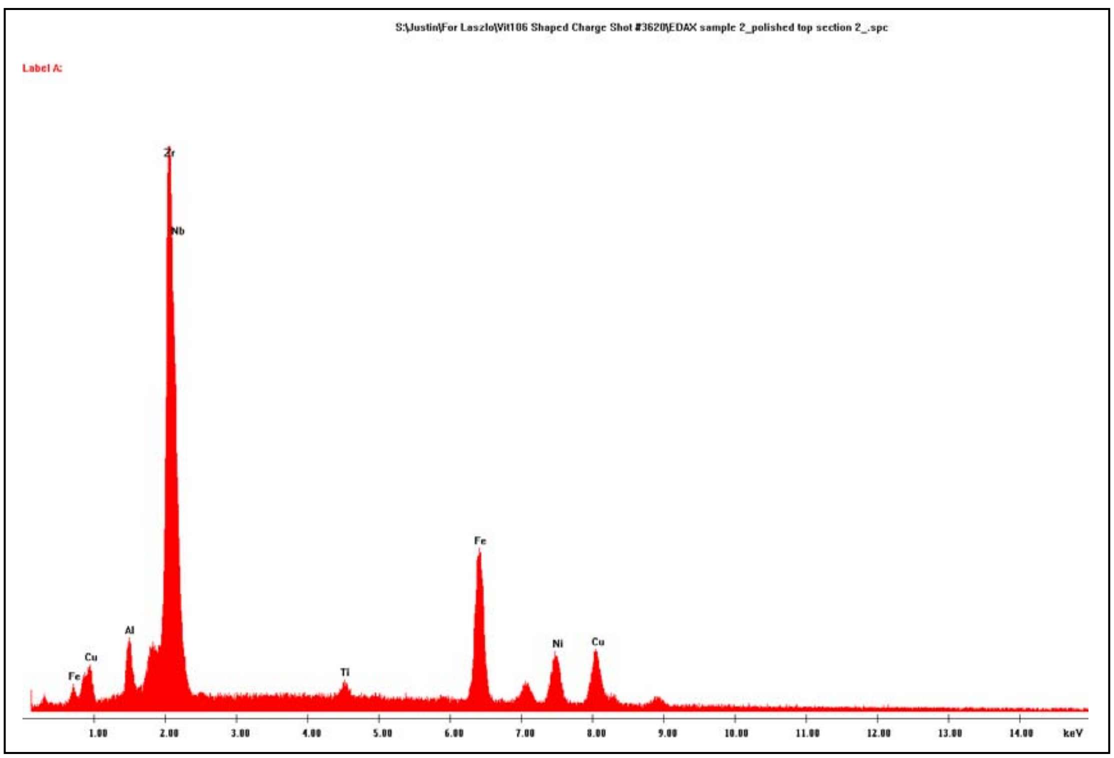

Figure 26. Secondary electron micro graph of a subsurface region of the A-2 witness plate displayed in figure 24, with the corresponding energy dispersive X-ray spectroscopic analyses for penetrating Vitreloy 106 alloy.

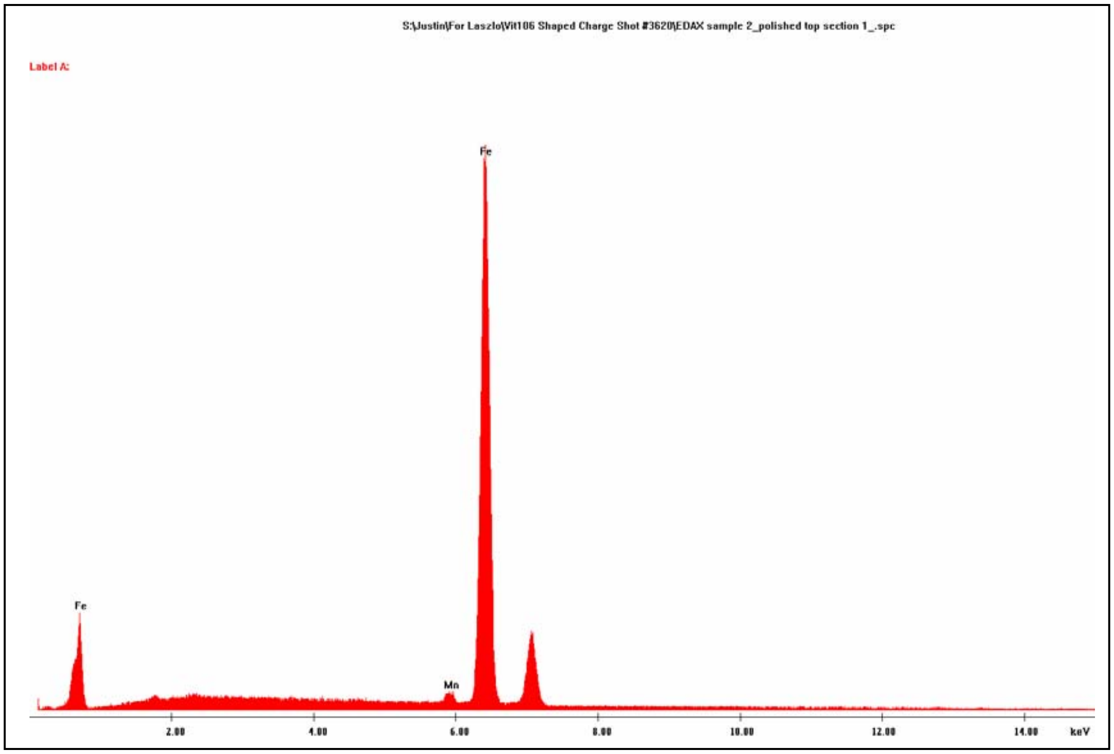

Figure 27. Secondary electron micro graph of a subsurface region of the A-2 witness plate displayed in figure 24, with the corresponding energy dispersive X-ray spectroscopic analyses for the steel substrate.

Similar examination of a section from the A-3 witness plate shows the intermixing of the steel with the molten metallic glass. Figures 28 and 29 illustrate that in this region, the bulk metallic glass, alloyed more with iron from the steel plate, is in a completely devitrified state. This is quite expected because even though the required high cooling rates may be present on the free surface to quench into an amorphous state, the shift away from the intended alloy composition would likely degrade the alloy's glass-forming ability. Note that the dissolution of the iron from the steel would lower the melting point of the metallic glass. The higher magnification image reveals a heterogeneous, interpenetrating dendritic structure. Additional images of the A-8 witness plate in figures 30 through 32 further exemplify that the dendritic regions are strongly affected by the composition and local cooling rates. It is purely speculative, but the dendrites in figure 31 most likely nucleated on the central particle cluster and the undercooling, required for solidification, was such that they could grow to fairly large dimensions. In contrast, closer to the steel plate (see figure 32), cooling was faster; therefore, the crystal size is somewhat smaller and more equiaxed.

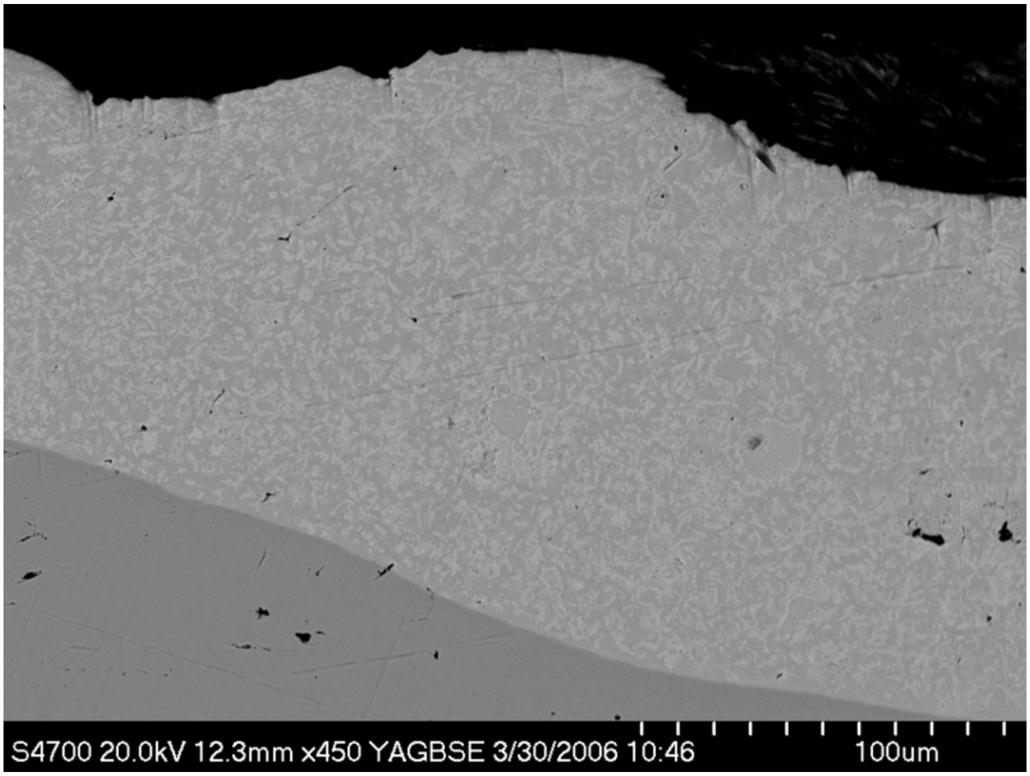

Figure 28. Backscattered electron micro graph of a surface region on the A-3 witness plate from appendix A is displayed.

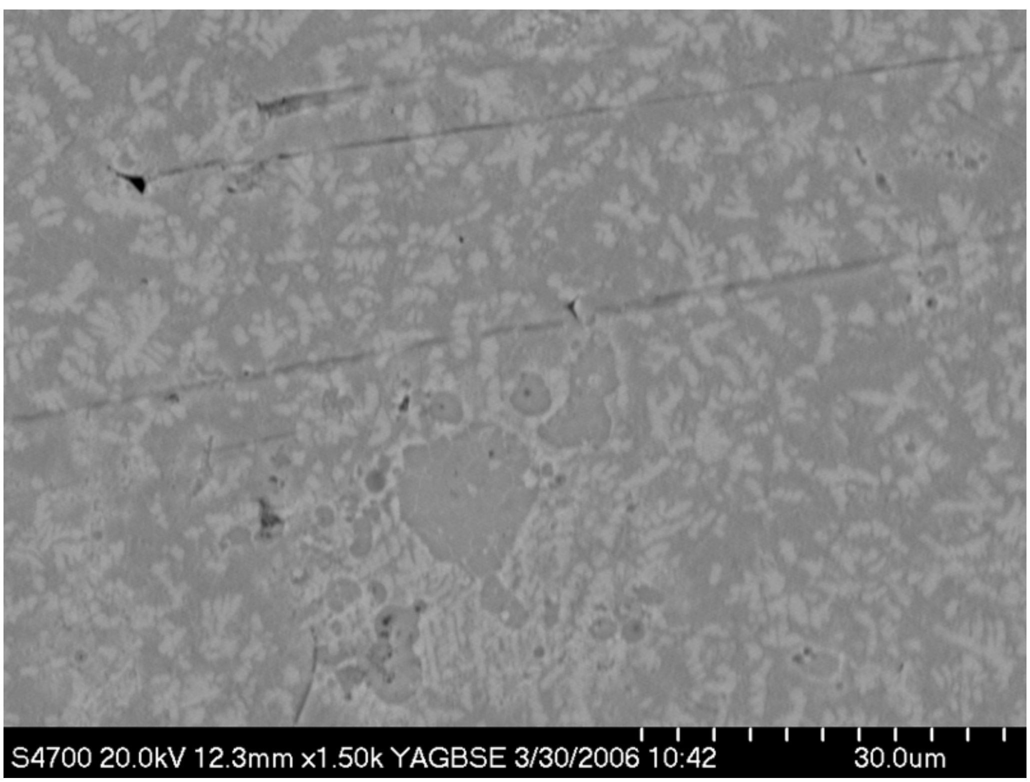

Figure 29. Backscattered electron micro graph of a surface region on the A-3 witness plate from appendix A is displayed with a higher magnification image of the fine structure.

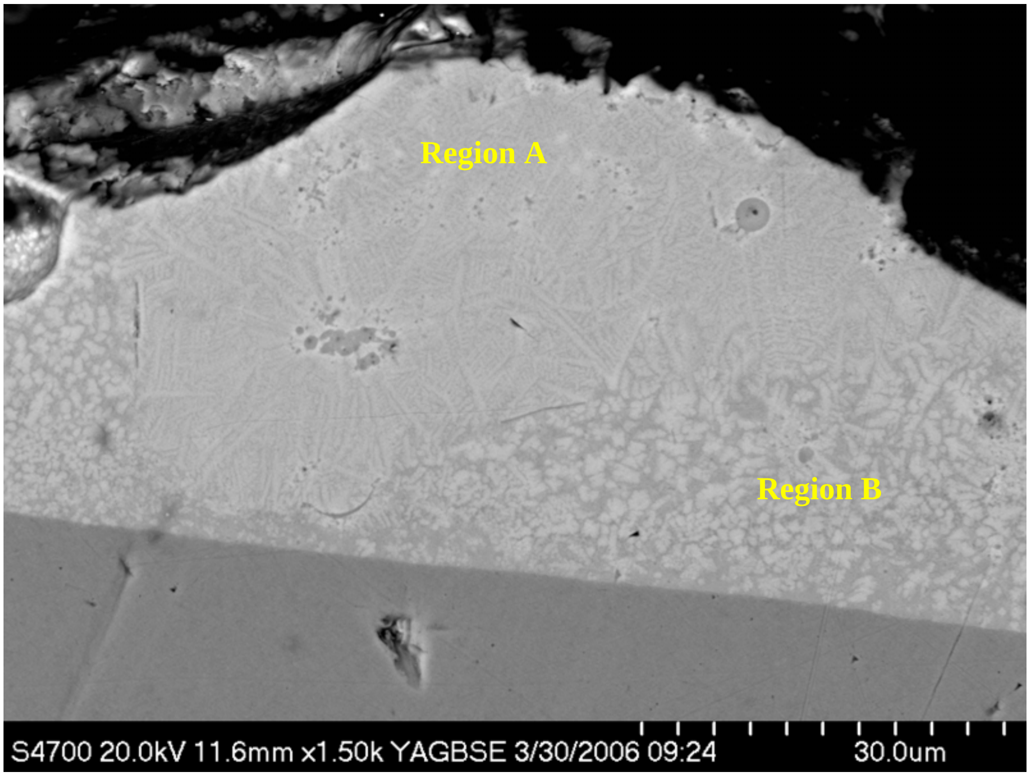

Figure 30. Backscattered electron micro graph of a surface region on the A-8 witness plate is displayed.

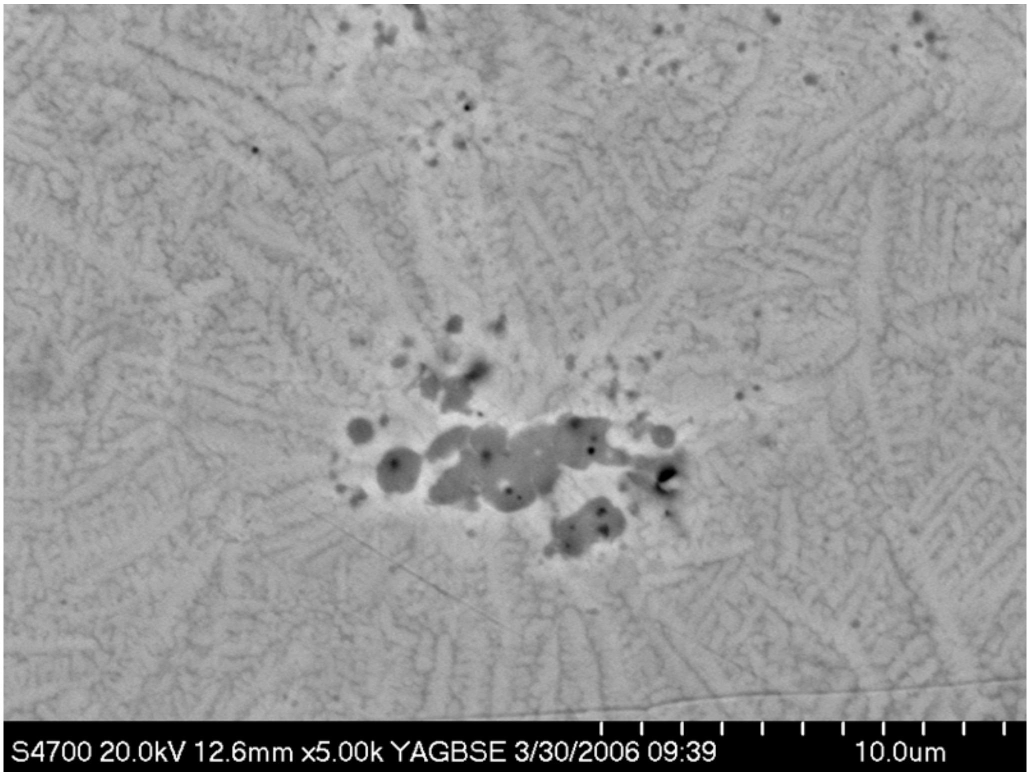

Figure 31. Backscattered electron micro graph of a surface region on the A-8 witness plate displayed in figure 30 with a higher magnification image of the fine structure from Region A.

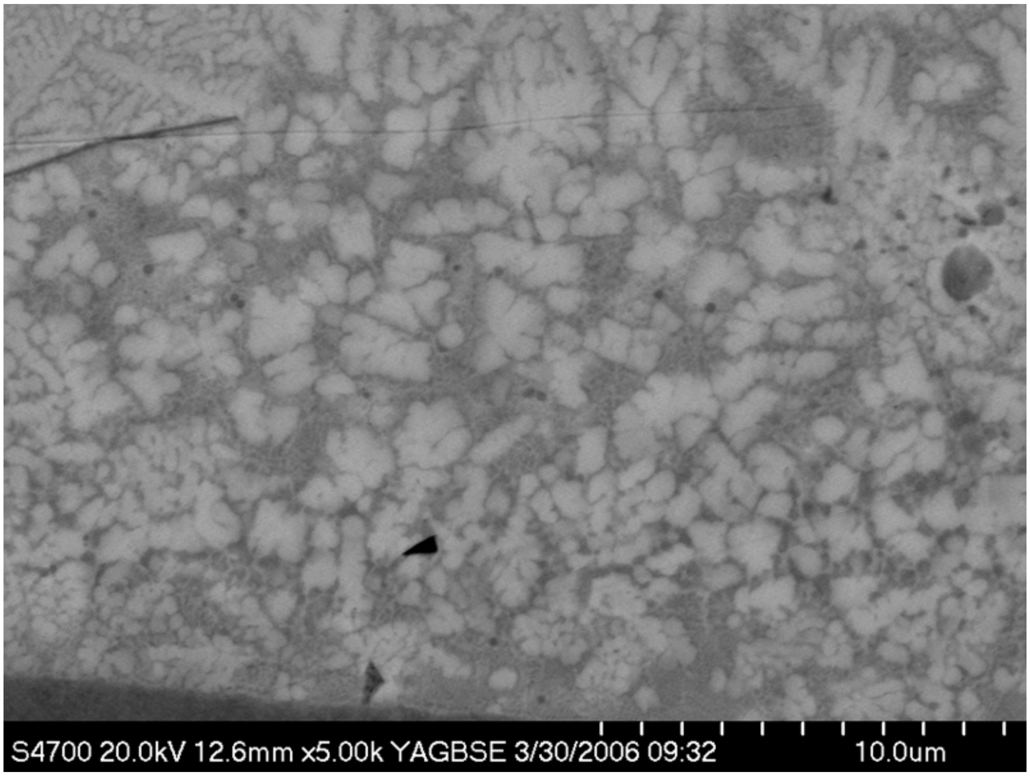

Figure 32. Backscattered electron micro graph of a surface region on the A-8 witness plate displayed in figure 30 with a higher magnification image of the fine structure from region B.

3.3 Erosion Mechanism of the Metallic Glass Liner Material

As revealed by flash X-ray radiographs and relatively poor penetration results in shots 3618 and 3619, it was surmised that the liner particulates in a highly nonuniform manner. This may be attributed to poor quality of the liner dimensions, trapped porosity, imprecise composition, and possibly high oxygen content. The high oxygen content of the liner is indicative that the as-cast liner was most likely not fully amorphous.

As was seen in shot 3620, when the distance between the detonating charge and target was reduced, penetration effectiveness improved. The smooth surface of the penetration tunnel from shot 3620 indicated that unlike the long stand-off scenarios of shots 3618 and 3619, the erosion by the dispersed jet was more effective. Figure 33 illustrates a fine channel generated by a metallic glass particle penetrating into the steel target plate. The atomic number contrast in the channel is indicative of post-penetration alloying of the metallic glass with steel.

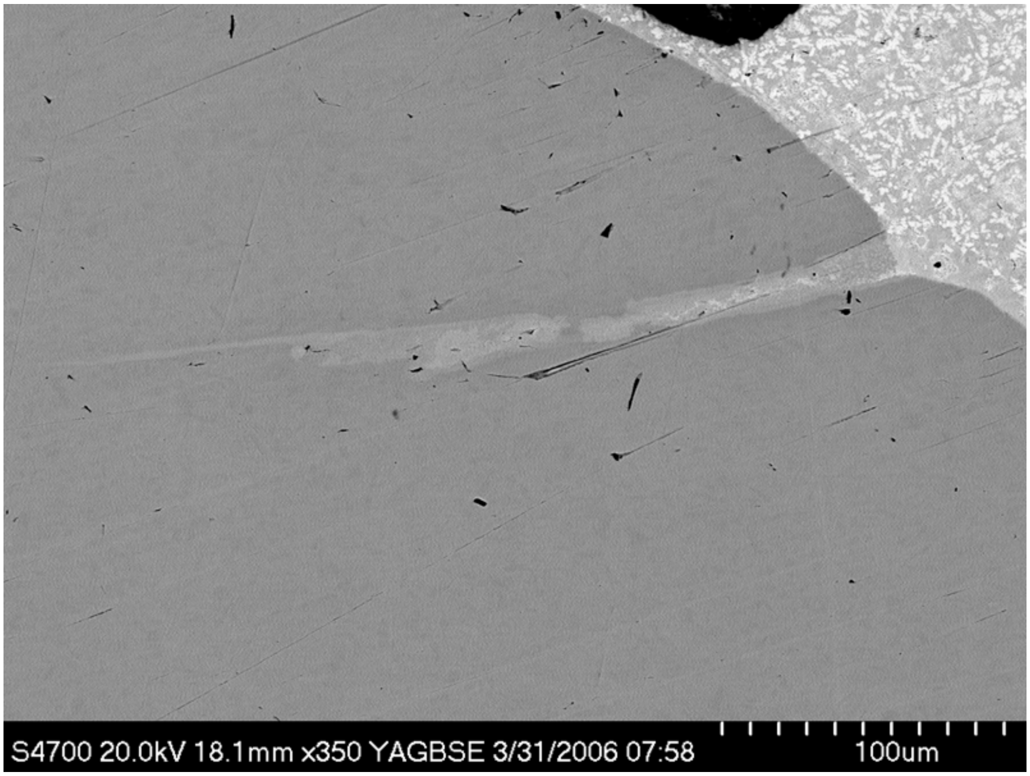

Figure 33. Backscattered electron micro graph of a surface region on the A-8 witness plate, from appendix A, showing penetration of the steel.

4. Conclusions

An experimental study was conducted to evaluate the effectiveness of a bulk metallic glass as a shaped charge liner. Results show that the zirconiam-based Vitreloy 106 liner behaved similar to particulating jets made from pressed powder liner materials. It was found that the liners were non-precision quality which contributed to their unremarkable performance. Jet formation was asymmetric and the particles in the jet were nonuniform in size and dispersion.

These preliminary tests revealed key aspects of the fundamental penetration behavior of bulk metallic glasses in a shaped charge configuration. The interaction between the metallic glass and steel plate is undergoing continued investigation. Similarly, additional tests with higher quality liners including better dimensional tolerances, alternate geometries (to subject the liner to lower strains, strain rates, pressure, and temperature) and lower impurity levels are being considered.

5. References

1. Hao Li, unpublished results, Michigan Technological University, Houghton, MI, July 2005.

2. Walters, W. P.; Zukas, J. Fundamentals of Shaped Charges, CMC Press, Baltimore, MD, 1998.

3. Walters, W. P.; Peregino, P.; Summers, R.; Leidel, D. *A Study of Jets From Unsintered-Powder Metal Lined Nonprecision Small-Caliber Shaped Charges*; ARL-TR-2391; U.S. Army Research Laboratory: Aberdeen Proving Ground, MD, February 2001.

4. Howmet Corporation, now a division of ALCOA, private communication, Whitehall, MI, no date.

5. Johnson, W. L. Bulk Glass-Forming Metallic Alloys: Science and Technology, *MRS Bulletin* **October 1999**, *24* (10), 42-56.

INTENTIONALLY LEFT BLANK.

Appendix A. Close View of Each of the Witness Plates

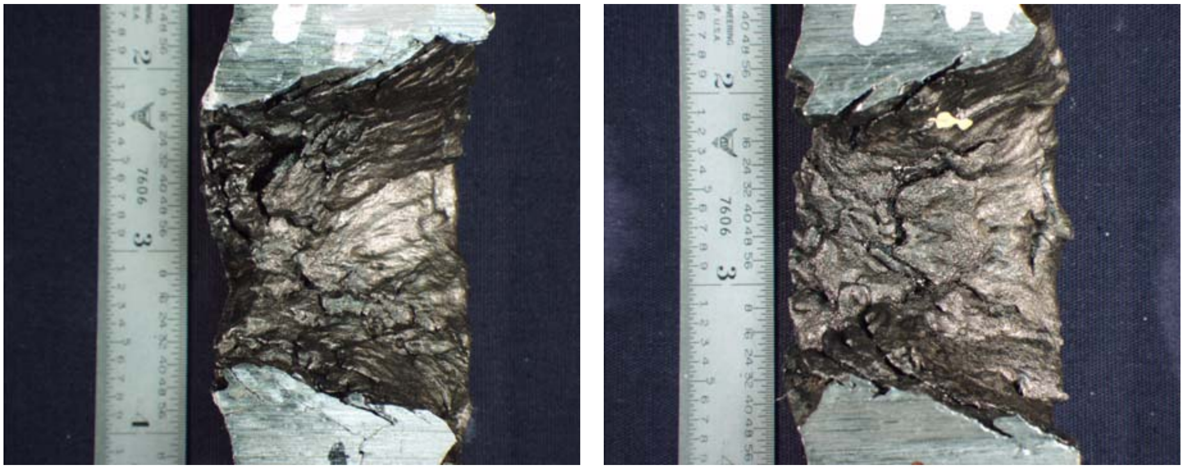

Figure A-1. Matching halves of the cross-sectional view of the first witness plate.

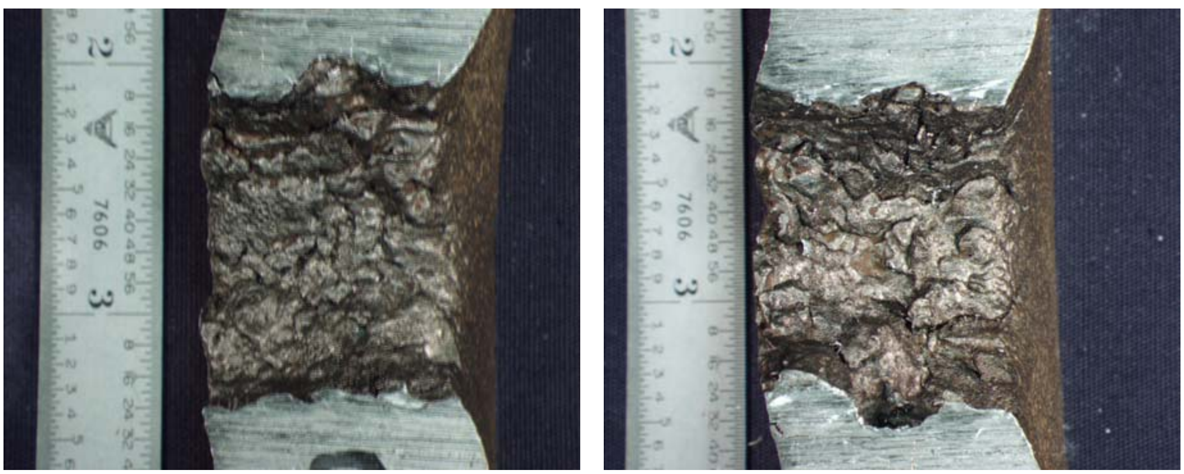

Figure A-2. Matching halves of the cross-sectional view of the second witness plate.

Figure A-3. Matching halves of the cross-sectional view of the third witness plate.

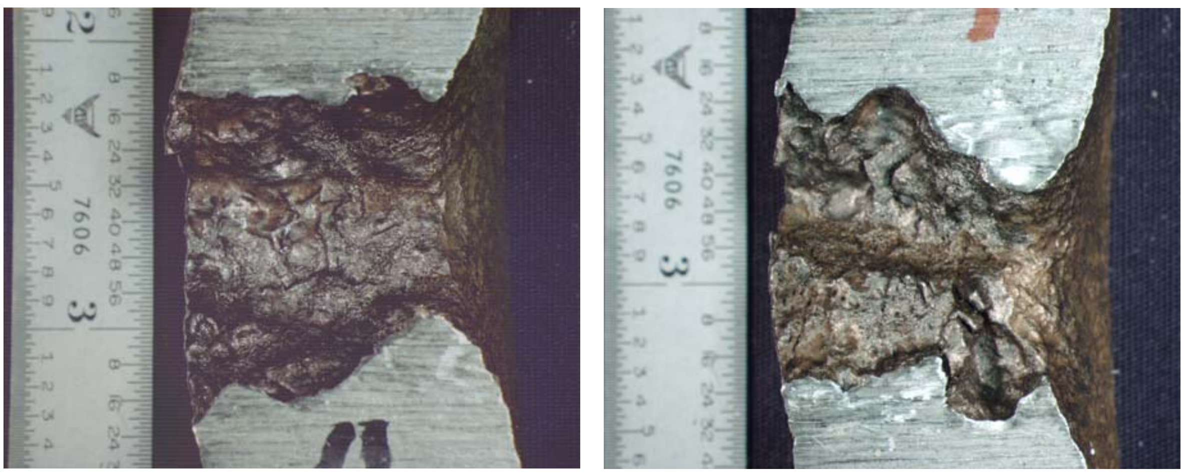

Figure A-4. Matching halves of the cross-sectional view of the fourth witness plate.

Figure A-5. Matching halves of the cross-sectional view of the fifth witness plate.

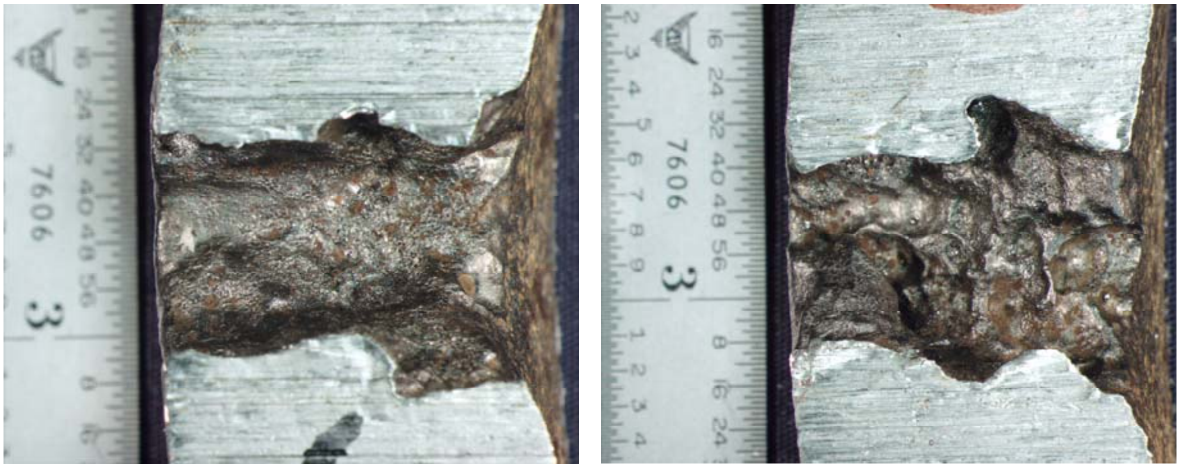

Figure A-6. Matching halves of the cross-sectional view of the sixth witness plate.

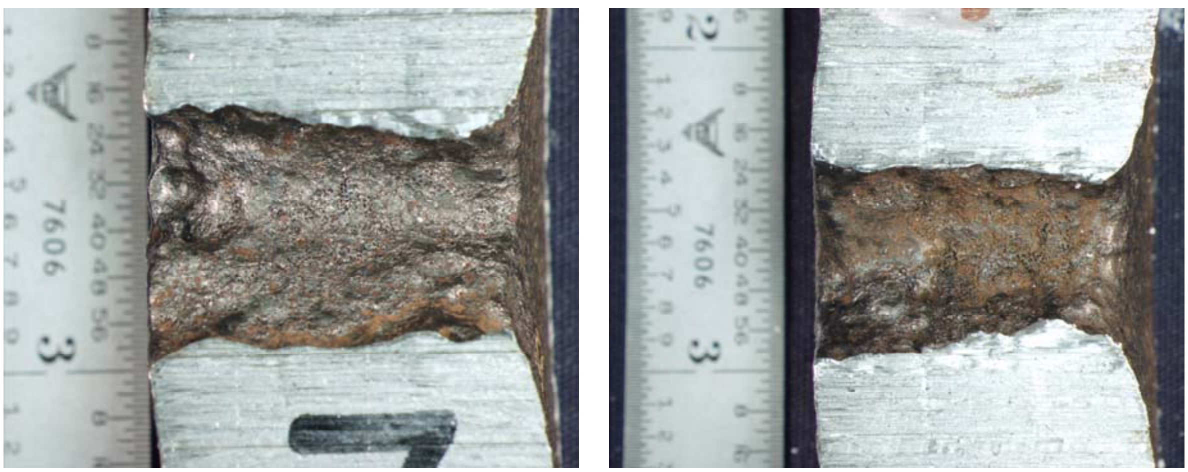

Figure A-7. Matching halves of the cross-sectional view of the seventh witness plate.

Figure A-8. Matching halves of the cross-sectional view of the eighth witness plate.

Figure A-9. Matching halves of the cross-sectional view of the ninth witness plate.

NO. OF COPIES	ORGANIZATION
1 (PDF ONLY)	DEFENSE TECHNICAL INFORMATION CTR DTIC OCA 8725 JOHN J KINGMAN RD STE 0944 FORT BELVOIR VA 22060-6218
1	US ARMY RSRCH DEV & ENGRG CMD SYSTEMS OF SYSTEMS INTEGRATION AMSRD SS T 6000 6TH ST STE 100 FORT BELVOIR VA 22060-5608
1	INST FOR ADVNCD TCHNLGY THE UNIV OF TEXAS AT AUSTIN 3925 W BRAKER LN STE 400 AUSTIN TX 78759-5316
1	DIRECTOR US ARMY RESEARCH LAB IMNE ALC IMS 2800 POWDER MILL RD ADELPHI MD 20783-1197
1	DIRECTOR US ARMY RESEARCH LAB AMSRD ARL CI OK TL 2800 POWDER MILL RD ADELPHI MD 20783-1197
2	DIRECTOR US ARMY RESEARCH LAB AMSRD ARL CS OK T 2800 POWDER MILL RD ADELPHI MD 20783-1197
1	OFC OF NAVAL RESEARCH J CHRISTODOULOU ONR CODE 332 800 N QUINCY ST ARLINGTON VA 22217-5600
1	DARPA L CHRISTODOULOU 3701 N FAIRFAX DR ARLINGTON VA 22203-1714
4	NIST F BIANCANIELLO S RIDDER S MATES 100 BUREAU DR GAITHERSBURG MD 20899

NO. OF COPIES	ORGANIZATION
1	GA TECH RESEARCH INST GA INST OF TCHNLGY N THADHANI ATLANTA GA 30392
3	CDR US ARMY ARDEC AMSTA AR WEE C E BAKER A DANIELS R FONG B3022 PICATINNY ARSENAL NJ 07806-5000
2	CDR US ARMY AVN & MISSILE CMD AMSAM RD PS WF S CORNELIUS S HOWARD REDSTONE ARSENAL AL 35898-5247
3	CDR US ARMY RESEARCH OFFFICE S F DAVIS K IYER A RAJENDRAN PO BOX 12211 RTP NC 27709-2211
1	CDR NAVAL WEAPONS CTR N FASIG CODE 3261 CHINA LAKE CA 93555
1	CDR NAVL SURFACE WARFARE CTR DAHLGREN DIVISION W E HOYE G22 17320 DAHLGREN RD DAHLGREN VA 22448-5100
4	CDR NAVL SURFACE WARFARE CTR DAHLGREN DIVISION R GARRETT G22 T SPIVAK G22 P WALTER F ZERILLI 17320 DAHLGREN RD DAHLGREN VA 22448-5100
1	AIR FORCE ARMAMENT LAB AFATL DLJR D LAMBERT EGLIN AFB FL 32542-6810
3	DARPA L CHRISTODOULOU W SNOWDEN S WAX 3701 N FAIRFAX DR ARLINGTON VA 22203-1714

NO. OF COPIES	ORGANIZATION
2	LOS ALAMOS NATL LAB P HOWE MS P915 J KENNEDY MS P915 PO BOX 1663 LOS ALAMOS NM 87545
1	LOS ALAMOS NATL LAB L HULL MS A133 PO BOX 1663 LOS ALAMOS NM 87545
2	SANDIA NATL LAB DOCUMENT PROCESSING MS0617 R BELL MS0836 9116 D CRAWFORD MS0836 9116 PO BOX 5800 ALBUQUERQUE NM 87185-0100
3	SANDIA NATL LAB DOCUMENT PROCESSING MS0617 E HERTEL MS0836 9116 S SILLING MS0820 9232 D PRECE MS 0819 PO BOX 5800 ALBUQUERQUE NM 87185-0100
3	DIR LLNL D BAUM L099 M MURPHY C SIMONSON MS PO BOX 808 MS L35 LIVERMORE CA 94550
2	SOUTHWEST RSCH INST C ANDERSON J WALKER PO DRAWER 28510 SAN ANTONIO TX 78228-0510
2	AEROJET J CARLEONE S KEY PO BOX 13222 SACRAMENTO CA 95813-6000
1	ALLIANT TECHSYSTEMS INC R TOMPKINS 5050 LINCOLN DR EDINA MN 55436
1	CMPTNL MECHS CNSLTNTS J A ZUKAS PO BOX 11314 BALTIMORE MD 21239-0314

NO. OF COPIES	ORGANIZATION
3	DETK R CICCARELLI W FLIS M MAJERUS 3620 HORIZON DR KING OF PRUSSIA PA 19406
1	TEXTRON DEFENSE SYSTEMS C MILLER 201 LOWELL ST WILMINGTON MA 01887-4113
1	D R KENNEDY & ASSOC INC D KENNEDY PO BOX 4003 MOUNTAIN VIEW CA 94040
1	LOCKHEED MARTIN ELECTRONICS & MISSILES G W BROOKS 5600 SAND LAKE RD MP 544 ORLANDO FL 32819-8907
4	GD OTS C ENGLISH T GRAHAM D A MATUSKA J OSBORN 4565 COMMERCIAL DR A NICEVILLE FL 32578
2	GD OTS D BOEKA N OUYE 2950 MERCED ST SUITE 131 SAN LEANDRO CA 94577
1	ZERNOW TECHNICAL SVS INC L ZERNOW 425 W BONITA AVE STE 208 SAN DIMAS CA 91773
1	PM JAVELIN PO SSAE FS AM EG C ALLEN REDSTONE ARSENAL AL 35898-5720
1	PM TOW SFAE TS TO J BIER REDSTONE ARSENAL AL 35898-5720

NO. OF COPIES	ORGANIZATION
1	HALLIBURTON ENERGY SVCS JET RESEARCH CENTER D LEIDEL PO BOX 327 ALVARADO TX 76009-9775
1	DIR LLNL R VAROSH L149 PO BOX 808 LIVERMORE CA 90550
3	INST FOR ADVNCD TECH S BLESS H FAN W REINECKE 3925 W BRAKER LN STE 400 AUSTIN TX 78759-5316
1	NORTHROP GRUMMAN DR D PILLASCH B57 D3700 PO BOX 296 1100 W HOLLYVALE ST AZUSA CA 91702
1	INTRNTL RSRCH ASSOC D ORPHAL 4450 BLACK AVE PLEASANTON CA 94566-6105
1	JIM VAROSH TELEDYNE RISI INC PO BOX 359 TRACY CA 95378

ABERDEEN PROVING GROUND

NO. OF COPIES	ORGANIZATION
1	DIRECTOR US ARMY RSCH LABORATORY ATTN AMSRD ARL CI OK (TECH LIB) BLDG 4600
45	DIR USARL AMSRL WM E SCHMIDT J SMITH AMSRL WM M S McKNIGHT R DOWDING AMSRL WM MB L BURTON W DRYSDALE W DEROSSET L KECSKES (15 CPS) M STAKER R WOODMAN ARSRD ARL WM MD J ADAMS E CHIN AMSRL WM T T HAVEL AMSRL WM TA M BURKINS W GOOCH M KEELE J RUNYEON AMSRL WM TB P BAKER J STARKENBERG R BANTON AMSRL WM TC R ANDERSON G BOYCE R COATES T FARRAND M FERMEN-COKER K KIMSEY L MAGNESS D SCHEFFLER S SCHRAML B SCHUSTER B SORENSEN R SUMMERS C WILLIAMS A. SIEGFRIED W WALTERS (6 CPS) AMSRL WM TD T BJERKE Y HUANG E RAPACKI T WEERASOORIYA S SEGLETES M RAFTENBERG AMSRD-ARL-SL-BE A PRAKASH

NO. OF COPIES	ORGANIZATION
1	TNO DEFENSE SECURITY & SAFETY E. CARTON LANGE KLEIWEG 137 P.O. BOX 45 2280 AA RIJSWIJK THE NETHERLANDS